Cell Reports

Article

Dynamic adoption of anergy by antigen-exhausted CD4$^+$ T cells

Graphical Abstract

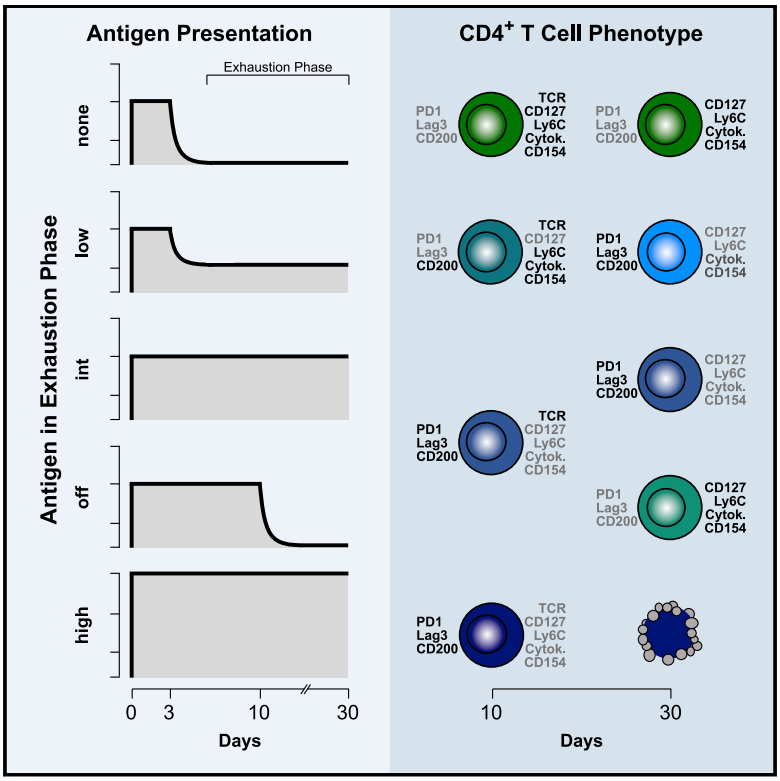

Highlights

- Th1 functionalities are reduced by persisting antigen in dose- and time-dependent manner
- Signaling pathways are adjusted to persisting antigen with different sensitivities
- Gene transcription is dynamically and reversibly adjusted to persisting antigen
- About half of the genes affected by antigen persistence respond in a dose-specific manner

Authors

Anne Trefzer, Pallavi Kadam, Shu-Hung Wang, ..., Johannes Beckers, Tobias Straub, Reinhard Obst

Correspondence

reinhard.obst@med.uni-muenchen.de

In Brief

In a system with regulatable antigen presentation *in vivo*, Trefzer et al. find TCR signaling, gene transcription, and functionalities reversibly regulated by dose and time of chronically persisting antigen. Comparisons with naturally anergic and tumor-infiltrating T cells suggest that signatures of anergy and exhaustion by antigen largely overlap.

Trefzer et al., 2021, Cell Reports *34*, 108748
February 9, 2021
https://doi.org/10.1016/j.celrep.2021.108748

CellPress

Cell Reports

CellPress
OPEN ACCESS

Article

Dynamic adoption of anergy by antigen-exhausted CD4$^+$ T cells

Anne Trefzer,[1,7] Pallavi Kadam,[1] Shu-Hung Wang,[1,8] Stefanie Pennavaria,[1] Benedikt Lober,[1,9] Batuhan Akçabozan,[1] Jan Kranich,[1] Thomas Brocker,[1] Naoko Nakano,[2] Martin Irmler,[3] Johannes Beckers,[3,4,5] Tobias Straub,[6] and Reinhard Obst[1,10,*]

[1]Institute for Immunology, Biomedical Center, Medical Faculty, Ludwig-Maximilians-Universität München, 82152 Planegg-Martinsried, Germany
[2]Research Institute for Biomedical Sciences, Tokyo University of Science, Chiba 278-0022, Japan
[3]Institute of Experimental Genetics, Helmholtz Zentrum München GmbH, 85764 Neuherberg, Germany
[4]Chair of Experimental Genetics, Technische Universität München, 85354 Freising, Germany
[5]German Center for Diabetes Research (DZD e. V.), Neuherberg, Germany
[6]Bioinformatics Core Facility, Biomedical Center, Medical Faculty, Ludwig-Maximilians-Universität München, 82152 Planegg-Martinsried, Germany
[7]Present address: Roche Innovation Center Zurich, Roche Glycart AG, 8952 Schlieren, Switzerland
[8]Present address: Center of Allergy and Environment, Technical University of Munich and Helmholtz Zentrum München GmbH, 80802 Munich, Germany
[9]Present address: Pharma Biotech Penzberg, Roche Diagnostics GmbH, 82377 Penzberg, Germany
[10]Lead contact
*Correspondence: reinhard.obst@med.uni-muenchen.de
https://doi.org/10.1016/j.celrep.2021.108748

SUMMARY

Exhausted immune responses to chronic diseases represent a major challenge to global health. We study CD4$^+$ T cells in a mouse model with regulatable antigen presentation. When the cells are driven through the effector phase and are then exposed to different levels of persistent antigen, they lose their T helper 1 (Th1) functions, upregulate exhaustion markers, resemble naturally anergic cells, and modulate their MAPK, mTORC1, and Ca^{2+}/calcineurin signaling pathways with increasing dose and time. They also become unable to help B cells and, at the highest dose, undergo apoptosis. Transcriptomic analyses show the dynamic adjustment of gene expression and the accumulation of T cell receptor (TCR) signals over a period of weeks. Upon antigen removal, the cells recover their functionality while losing exhaustion and anergy markers. Our data suggest an adjustable response of CD4$^+$ T cells to different levels of persisting antigen and contribute to a better understanding of chronic disease.

INTRODUCTION

T cells faced with chronic infections and cancer are prone to become dysfunctional due to the persistence of antigen, inflammation, and debilitating microenvironments. Virus-induced exhaustion of CD8$^+$ T cells has suggested a differentiation program affected by multiple checkpoint inhibitors (Hashimoto et al., 2018; McLane et al., 2019). Although they are central to fighting infections and cancer directly, and indirectly by CD8$^+$ T and B cells (Borst et al., 2018; Haabeth et al., 2014; Laidlaw et al., 2016), much less is known about CD4$^+$ T cell responses to chronic stimulation. Because they are, by and large, more flexible in their responses to antigen than CD8$^+$ T cells (Nguyen et al., 2019; Obst, 2015), diverse responses to chronic infections and cancer can be expected. Altered CD4$^+$ T cell functionalities have been described in patients chronically infected with HIV and hepatitis C virus (HCV) (Morou et al., 2019; Raziorrouh et al., 2016; Schulze zur Wiesch et al., 2012). CD4$^+$ T cells reacting to the chronic LCMV cl13 (lymphocytic choriomeningitis virus clone 13) variant are critically important for the late clearance of the virus (Aubert et al., 2011; Harker et al., 2011; Zander et al., 2019) by enhancing humoral and cytotoxic responses via interleukin-21 (IL-21) (Fahey et al., 2011; Greczmiel et al., 2017; Vella et al., 2017). On the other hand, LCMV-reactive CD4$^+$ T cells share signs of dysfunctionality, such as an impaired T helper 1 (Th1) phenotype, with their CD8$^+$ counterparts (Brooks et al., 2005; Crawford et al., 2014; Fuller and Zajac, 2003; Snell et al., 2016).

It is increasingly realized that CD4$^+$ T cells critically contribute to tumor surveillance directly and indirectly (Borst et al., 2018; Haabeth et al., 2014). For immunotherapy, the efficacy of eliciting CD8$^+$ T memory (Tmem) cell responses has been assisted by raising CD4$^+$ responses simultaneously, bolstering cytotoxic T lymphocyte (CTL) numbers or conditioning tumors for attack, thus making the search for major histocompatibility complex class II (MHC class II)-restricted tumor neo-antigens a promising task in immuno-oncology (Alspach et al., 2019; Borst et al., 2018; Ferris et al., 2020). The observation that tumor mutations escaping MHC class II presentation are even more positively selected than those escaping MHC class I binding emphasize

the importance of Th cells in tumor editing and chronic disease in general (Pyke et al., 2018).

Mechanisms of T cell exhaustion include the expression of inhibitory receptors that are likely to protect from autoimmunity and immunopathology (Cornberg et al., 2013; McKinney et al., 2015; Oldstone et al., 2018), and immune-mediated side effects of checkpoint inhibitors confirm this notion (Quandt et al., 2020). Unresponsive, or anergic, T cells have been initially demonstrated by T cell receptor (TCR) stimulation (or "signal 1") alone but have also been identified *in vivo* (Chappert and Schwartz, 2010; Kalekar et al., 2016). Data suggest that they exhibit altered TCR signaling with incomplete AP-1 (activator protein 1) and thus "unpartnered" NFAT (nuclear factor of activated T cells) transactivation and transcriptomically resemble exhausted T cells (Martinez et al., 2015), although altered TCR signaling in exhausted T cells has rarely been addressed (Ebert et al., 2016; Han et al., 2010; Sandu et al., 2020; Staron et al., 2014; Verma et al., 2021). Conceptually, anergic cells differ from exhausted ones in that their primary stimulation has been incomplete, while the latter have been primed successfully but then lose their functionality. However, it is possible that T effector (Teff) cells confronted with persisting antigen become exhausted and increasingly similar to anergic cells.

To better understand antigen-driven exhaustion of $CD4^+$ T cells in relation to anergy, we here analyze their differentiation in a sterile system of regulated antigen presentation. To establish chronic infections in mouse models, the immune response has to be overwhelmed from the beginning by high pathogen loads, which then continue to exhaust the T cells, raising issues of causality (Frebel et al., 2010; Li et al., 2009). The high-dose LCMV cl13 and Docile models have been informative (Hashimoto et al., 2018; McLane et al., 2019), but it is unclear how good a model they are for human infections and malignancies. In the system used here, $CD4^+$ T cells are primed uniformly and are then exposed to different antigen doses that deviate them to different phenotypes. The absence of confounding innate responses to pathogens, with their own mechanisms of training, resistance, and tolerance, allows for a reductionist analysis of $CD4^+$ T cell exhaustion driven by antigen alone persisting at different levels. We here report the dynamic regulation of Th1 functionality, TCR signaling capacity, and gene expression in an antigen-dose- and time-dependent manner; define similarities to naturally anergic $CD73^+$folate receptor 4^+ ($FR4^+$) cells and to NFAT-induced, LCMV-exhausted, and tumor-infiltrating $CD4^+$ T cells; and probe the cells' ability to transmit help to B cells. The results dissect the effects of graded levels of antigen-mediated and reversible exhaustion. The finding that naturally anergic cells resemble antigen-exhausted ones suggests that a substantial proportion of $CD4^+$ T cells is anergized by persistent self-antigens or commensal antigens.

RESULTS

Different TCR signal strengths induced by increasing levels of antigen presentation *in vivo*

To investigate the effects of signal strength on $CD4^+$ T cell exhaustion *in vivo*, we have used a system in which the expression of the moth cytochrome *c* (MCC) peptide $MCC_{93–103}$ can be regulated in dendritic cells (DCs) for presentation in the context of H-$2E^k$. The inducible MCC (iMCC) recipients carry two transgenes, depicted in Figure 1A, which allow for doxycycline (dox)-dependent transcription of a modified *Cd74* cDNA that delivers the MCC peptide to the MHC class II processing pathway (Obst et al., 2005). In mice treated with 100 μg/mL dox, the reporter transgene is primarily expressed in conventional type 1 DCs (cDC1s) and plasmacytoid DC (pDCs), at about 20–40 times lower levels in cDC2 and macrophages (MPhs), and in B cells not at all, while a constitutively expressed Cd74-MCC transgene (cMCC; Yamashiro et al., 2002) is expressed at >20-fold higher levels and in all cell types analyzed (Figure 1B; Figure S1A). The $CD4^+$ T cell response to the $E^k/MCC_{93–103}$ epitope is dominated by cells carrying the Vα11/Vβ3 (TRAV4/TRBV26) TCR chains (Malherbe et al., 2008; Newell et al., 2011). Both transgenics (tgs) appear to be devoid of an endogenous E^k/MCC-reactive repertoire because no cells with an activated $CD44^{high}CD62L^{low}$ phenotype accumulate upon immunization above the adjuvant-induced background (Figure S1B), likely because of unresponsiveness or negative selection by neo-self MCC and perhaps assisted by *Aire*.

The AND TCR is representative of those recognizing the $E^k/MCC_{93–103}$ complex with high affinity because its exact CDR3α and β sequences have been re-identified among $CD4^+$ T cells responding to immunization; they also carry eight structurally preferred amino acids defined for efficient interaction (Kaye et al., 1989; Malherbe et al., 2008; Newell et al., 2011). Upon adoptive transfer into iMCC recipients fed with no dox, a low dose of dox, or a high dose of dox (0, 10, and 100 μg/mL, respectively) in the drinking water, AND TCR tg T cells responded accordingly by different degrees of proliferation. The cMCC recipients elicited an even higher and more homogeneous response (Figure 1C, left panels), likely because of high levels of antigen presentation by cDC1 (Figure 1B).

We noticed that about 80%–95% of the AND TCR molecules disappear from the cell surface in cMCC recipients, indicating a high level of antigen encountered there (Figure 1C, right panels). MCC presentation by B cells, however, was an unlikely cause of TCR downregulation for two reasons. First, AND T cells devoid of the signaling lymphocyte activation molecule-associated protein (SAP), which is necessary for the stable interaction of T and B cells (Qi et al., 2008), do downregulate their TCR just like wild-type (WT) cells with the TCR molecules are still detectable intracellularly (Figure 1D). Second, TCR downregulation was also found upon transfer of AND T cells into cMCC recipients lacking B cells because of a deleted *Rag2* gene (Figure S1C). These data indicated that TCR endocytosis from the cell surface in cMCC recipients is caused by a high level of MCC presentation by non-B APCs like DCs and MPhs.

The direct visualization of TCR signals via the NR4a1-EGFP transgene (Moran et al., 2011) and the CD69 activation marker showed full activation of the T cells at intermediate and high antigen doses 16 h posttransfer (pt), but only weak signs of signaling in iMCC recipients fed the low 10 μg/mL dose of dox (Figure 1E, left panels). Analyses at later time points, however, demonstrated that the cells became fully activated when stimulated for 2 days (Figure 1E, right panels), indicating the accumulation of at least one TCR signaling intermediate over time before

CellPress
OPEN ACCESS

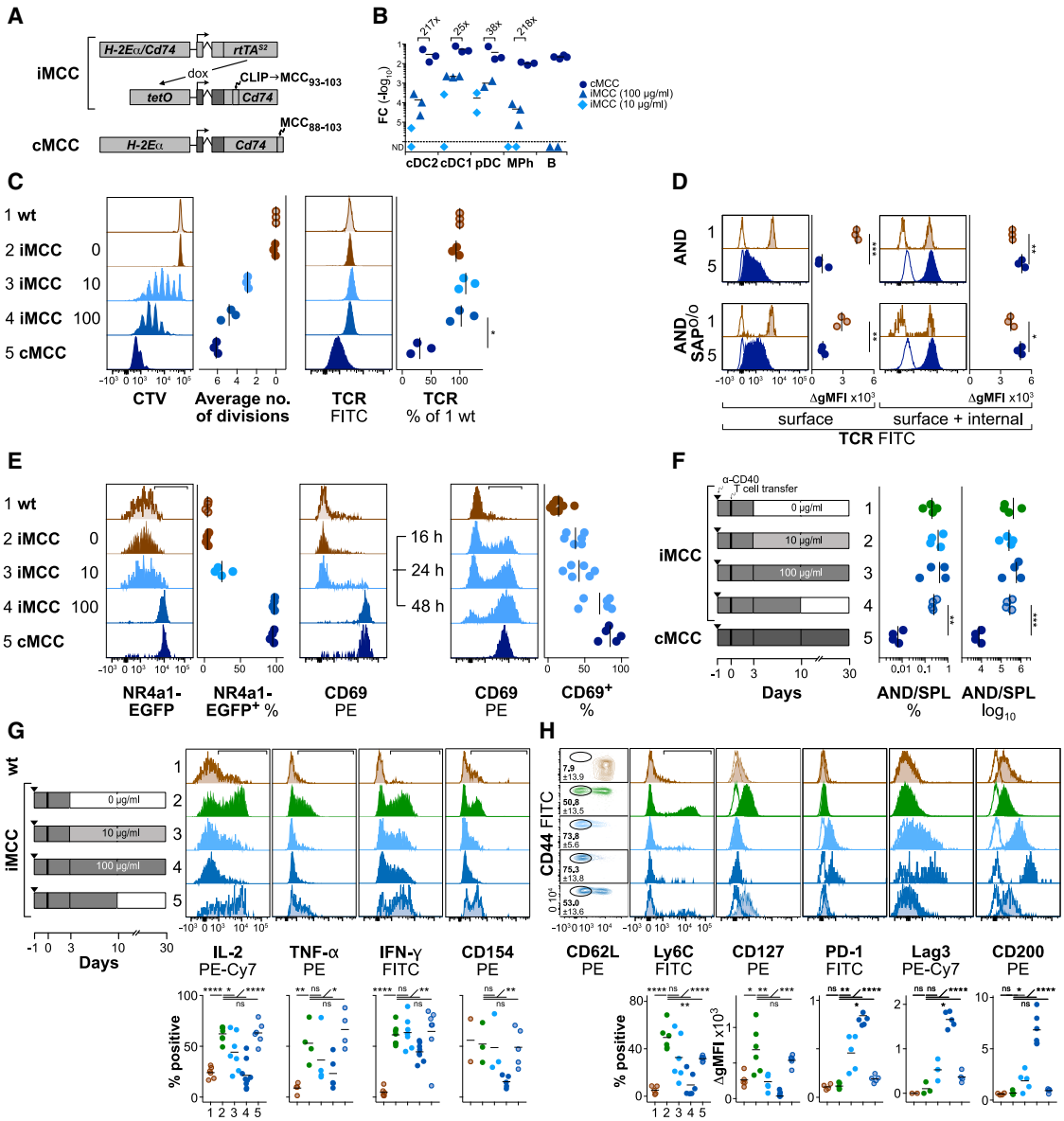

Figure 1. T cell exhaustion of CD4$^+$ AND T cells driven by regulated antigen presentation *in vivo*

(A) Schematic depiction of MCC-encoding transgenes. The iMCC line carries two transgenes for the dox-inducible presentation of the $MCC_{93–103}$ core epitope by H-2E^k: *Cd74* and *H-2Eα* regulatory elements drive the reverse tetracycline transactivator rtTA^{S2}, which in the presence of dox induces an $MCC_{93–103}$-modified *Cd74* cDNA. The cMCC construct consists of H-2Eα enhancer and promoter sequences with a *Cd74* cDNA and $MCC_{88–103}$ added on.

(B) Expression of the Cd74 transgenes by sorted APC populations, as shown in Figure S1A. The ratios of the means of cMCC:iMCC (100 μg/mL dox) are given on top. Data are compiled from three independent experiments with n = 2–4 animals per condition.

(C) Proliferation (left) and TCR surface expression (right) of CD4$^+$ AND TCR tg T cells in five recipients 2.5 days pt. iMCC tg animals were fed with 0, 10, and 100 μg/mL dox, beginning on day −1. Data are compiled from three independent experiments with n = 1 recipient per condition.

(D) TCR expression by AND and AND *SAP*$^{o/o}$ donor T cells in cMCC recipients 3 days pt. Data are from three independent experiments with n = 1 recipient per condition.

(E) NR4a1-EGFP reporter gene and CD69 expression by AND T cells transferred into the recipients listed on the left. Splenocytes were analyzed 16 h pt (left) and 16, 24, and 48 h pt (right). Data are compiled from four (left) and six (right) independent experiments with n = 1 recipient per condition.

(F) Numbers of AND T cells transferred into the recipients depicted on the left. All iMCC animals were treated intraperitoneally (i.p.) with an anti-CD40 monoclonal antibody (mAb) on day −1 (indicated in all schematics by an inverted triangle), fed with 100 μg/mL dox, and transferred with AND T cells on day 0. On day 3, the dox dose was switched to 0 (condition 1), 10 (condition 2), or left at the initial 100 μg/mL (conditions 3 and 4), one of which was taken off dox on day 10 (condition 4). Data are from four independent experiments with n = 1 recipient per condition.

(G and H) Expression of cytokines and CD154 upon restimulation (G) and memory and exhaustion markers (H) by AND T cells on day 10 pt. Data are compiled from two to six independent experiments with n = 1 recipient per condition.

*p < 0.05, **p < 0.005, ***p < 0.0005 (unpaired Student's t test).

See also Figure S1.

reaching a threshold for proliferation (Moreau and Bousso, 2014; Rachmilewitz and Lanzavecchia, 2002). In summary, these data evidenced that $CD4^+$ AND TCR tg T cells receive no, a low, an intermediate, or a high level of TCR stimulation in dox-fed iMCC and cMCC recipients.

Persistent antigen presentation compromises $CD4^+$ T cell functionality by day 10

To explore the role of different antigen doses in exhaustion, we made use of the observation that AND T cells transiently stimulated by antigen presented by CD40-activated DCs efficiently differentiate into Teff and Tmem cells if antigen is turned off 3 days pt (Obst et al., 2007). T cells also survived by day 30 pt when antigen persisted at low and intermediate levels or when it was removed 10 days pt, but hardly in cMCC animals (Figure 1G), suggesting apoptosis or deletion as an outcome of exhaustion driven by antigen at a high level. Chronically persisting antigen at the intermediate dose caused dysfunctionality regarding the synthesis of IL-2, tumor necrosis factor alpha (TNF-α), interferon (IFN)-γ, and expression of the stimulatory receptor CD40L (CD154; Figure 1H). Importantly, turning off the MCC antigen on day 10 pt reversed the expression of memory (Ly6C, CD127) and exhaustion markers (PD-1, Lag3, CD200) and the above cytokines, while antigen persisting at the low dose affected only some of them (Ly6C, CD127, CD200, Figure 1H; IL-2, Figure 1E). These data showed that $CD4^+$ T cells respond dynamically to antigen chronically persisting at three different levels. They also suggest that $CD4^+$ T cells readjust their phenotype to a reduced antigen load.

Because it has been observed that signs of exhaustion can be detected early in chronic T cell responses (Han et al., 2010; Mann and Kaech, 2019; Staron et al., 2014), we next asked how functionality is compromised by persisting antigen until day 10 pt, when AND T cells were still detectable in the high-dose recipients (Figure 2A). Although all antigen-exposed cell populations upregulated CD44 and lost the integrin CD62L, only those in the cMCC recipients, presenting the highest antigen dose, downregulated their TCR (Figure 2B). At the same time, the Tmem markers CD127 and Ly6C were found to be downregulated with increasing antigen dose, with CD127 being more sensitive (Figure 2B). Accordingly, the presence of MCC at intermediate and high dosages between days 3 and 10 compromised cytokine secretion and CD154 expression of the cells, whereas MCC persisting at the low dose had little effect on T cell functionality (Figure 2C). These results indicated that antigen persistence between days 5 and 10 compromises Teff cell differentiation to Tmem cells at intermediate and high doses. In addition, the data show that continuously antigen-exposed AND T cells show the core characteristics of exhausted T cells on both days 10 and 30.

Continuous TCR stimulation undermines signaling to a later challenge

The results above suggested that continued TCR triggering might affect its signaling pathways differentially and thereby contribute to clonal T cell exhaustion. We thus asked whether the cells are able to perceive persisting antigen by assessing first NR4a1 expression, which reflects signals triggered by the TCR, rather than cytokines and inflammatory mediators, and integrates signaling events mostly by the protein kinase C (PKC), mitogen-activated protein kinase (MAPK), and/or Ca^{2+} pathways (Zikherman et al., 2012). AND T cells carrying the tg NR4a1-EGFP reporter (Moran et al., 2011) were transferred into cMCC and iMCC recipients. iMCC animals were initially treated with 100 μg/mL dox for 3 days, before being switched to 0, 10, or 100 μg/mL dox in the drinking water. Dox withdrawal results in the loss of $E^k/MCC_{93–103}$ presentation within 2 days (Obst et al., 2005). On days 6 and 10, EGFP expression at intermediate and high doses reflected TCR signaling at a time when the cells exhibit signs of exhaustion (Figure 3A). In the recipients fed with 10 μg/mL dox, EGFP was found to be expressed above background by day 10, but not by day 6, hinting at signal accumulation toward exhaustion by consecutive interactions with one or several APCs over time, for which previous evidence exists in the context of priming (Celli et al., 2005; Faroudi et al., 2003; Henrickson et al., 2008). EGFP expression by AND T cells transferred into cMCC recipients indicated that the few TCR molecules at the surface, or internalized ones, are signaling via the PKC, MAPK, and/or Ca^{2+} pathways that can be read out by the NR4a1-EGFP reporter (Zikherman et al., 2012).

We next asked whether the Ca^{2+}/calcineurin pathway leading to the nuclear translocation of NFAT family members (Hogan et al., 2003) does contribute to the continued TCR signals in chronically antigen-exposed T cells. Adoptively transferred AND T cells were retrieved from the recipients on day 10, immediately fixed, and analyzed for nuclear NFATc1 (also known as NFAT2) translocation by imaging flow cytometry. The cells expressed similar overall levels of NFATc1 under all conditions, but its nuclear translocation correlated with the level of antigen presentation *in vivo* (Figure 3B). These data demonstrated that the Ca^{2+}/calcineurin pathway is continuously triggered and operative in antigen-exhausted $CD4^+$ T cells exhibiting signs of dysfunctionality. The high level of NFATc1 translocation at the highest dose, where TCR is mostly internalized, indicates that few TCR molecules at the surface or in an intracellular compartment are sufficient for signaling.

To explore what causes the dysfunctionality of the AND T cells faced with high levels of chronic antigen, we analyzed IFN-γ expression on day 10 pt. As before, TCR levels were found to be reduced (Figure 3C, left panels). IFN-γ production in response to the standard phorbol myristate acetate (PMA)/ionomycin (IM) restimulation was weakly reduced, indicating that TCR signaling downstream of diacylglycerol and PKC intermediates remained mostly intact. Restimulation with splenocytes and the $MCC_{93–103}$ peptide, however, did not trigger any IFN-γ synthesis (condition 3), compared with control cells differentiating toward Tmem cells in transiently treated iMCC recipients (condition 2; Figure 3C, left panels). An overnight culture of the $CD4^+$ T cells in the absence of APCs allowed for the TCR to be re-expressed at the cell surface to almost original levels. However, IFN-γ production in response to the peptide did not recover (Figure 3D, right panels), suggesting that acute TCR signaling in cMCC recipients becomes compromised proximally to the TCR and remains so, even after normalization of TCR surface expression. We indeed find *Lat* mRNA and protein downregulated (below), and it is possible that TCR signaling components like it are regulated transcriptionally and/or epigenetically.

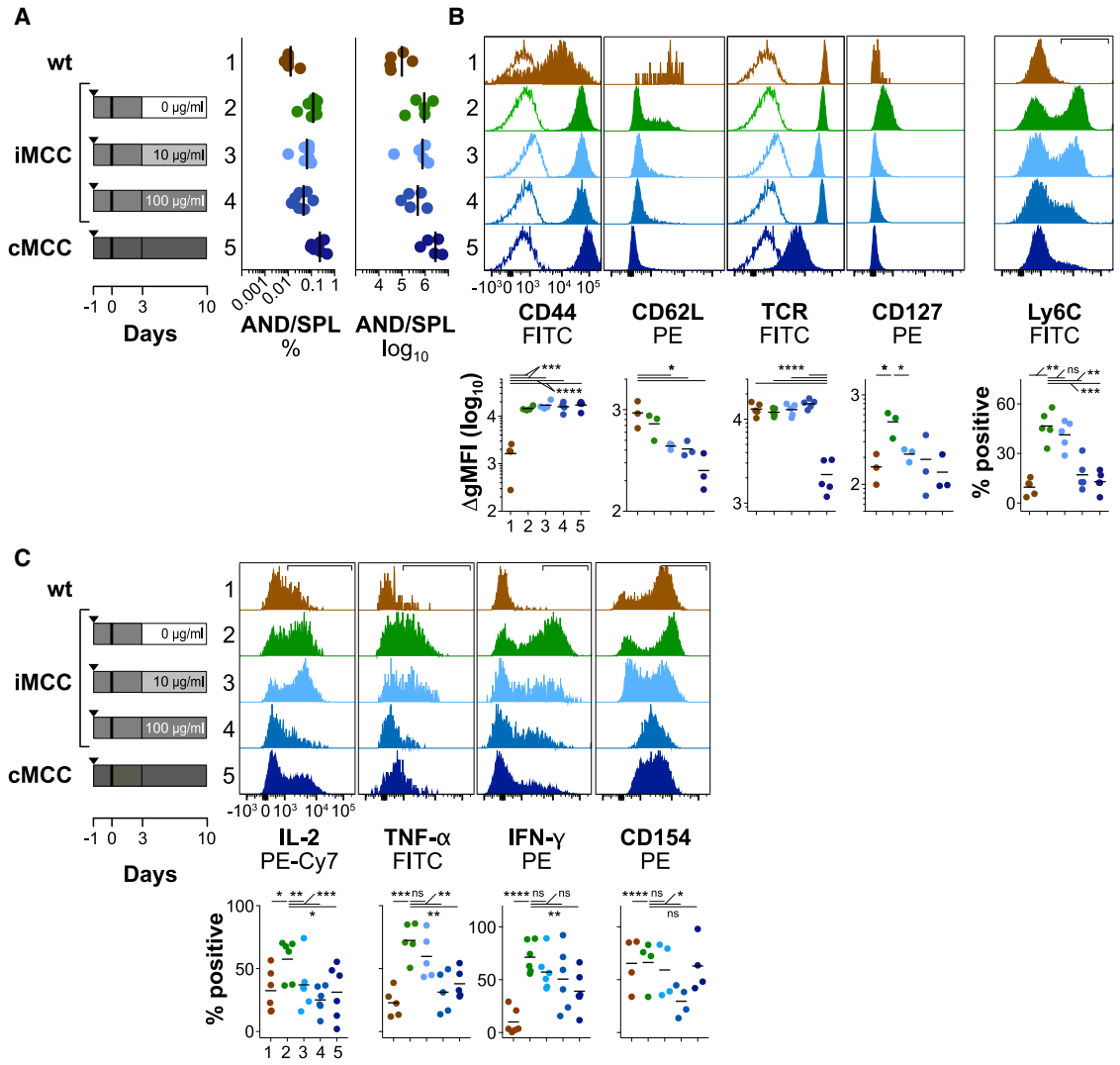

Figure 2. Phenotype and functionality of AND T cells following chronic antigen exposure at different doses

(A) Percentage and cell numbers of AND CD4$^+$ T cells found among splenocytes from recipients diagrammed on the left. Data are compiled from five independent experiments with n = 1 recipient per condition.

(B and C) Marker and cytokine expression by AND T cells 10 days pt. Data are from three to five independent experiments with n = 1 recipient per condition. *p < 0.05, **p < 0.005, ***p < 0.0005 (unpaired Student's t test).

We further explored the ability of rested cMCC-exhausted T cells to flux Ca^{2+} in response to acute TCR/CD4 crosslinking. The Ca^{2+} indicator tracings remained unresponsive to it, unlike those of control AND and endogenous CD4$^+$ T cells (Figure 3E). These results were corroborated *in vivo*, using AND T cells that were, following antigen exposure for 10 days in cMCC recipients, transferred into WT or cMCC secondary recipients. Two days later, the responses to TCR/CD4 crosslinking were not improved by the antigen-free environment, despite TCR re-expression at the surface (Figure 3F). These data indicated an irreversible damage of the Ca^{2+} response proximal to the TCR following chronic *in vivo* exposure to antigen at a high level. Because we had observed previously that T cells exhausted by antigen persisting at the intermediate level are able to robustly flux Ca^{2+} on day 10 (Han et al., 2010), we conclude that the types of exhaustion caused by antigen persisting at different doses are, at least partially, mediated by different molecular mechanisms. At this time point, only the high dose of chronic antigen compromised the Ca^{2+} response to *in vitro* TCR/CD4 crosslinking.

To assess the functionality of further pathways transmitting TCR signals in antigen-exhausted cells, we challenged adoptively transferred naive and antigen-exposed AND T cells on day 10 pt *in vivo* with an intravenous (i.v.) injection of the $MCC_{93–103}$ peptide. One hour later, the phosphorylation of the ribosomal protein S6, indicative of mTORC1 (mechanistic target of rapamycin complex 1) activity, was reduced in a subset of cells exhausted by intermediate antigen levels and in virtually all of them in cMCC recipients (Figure 3G, left panels). We then

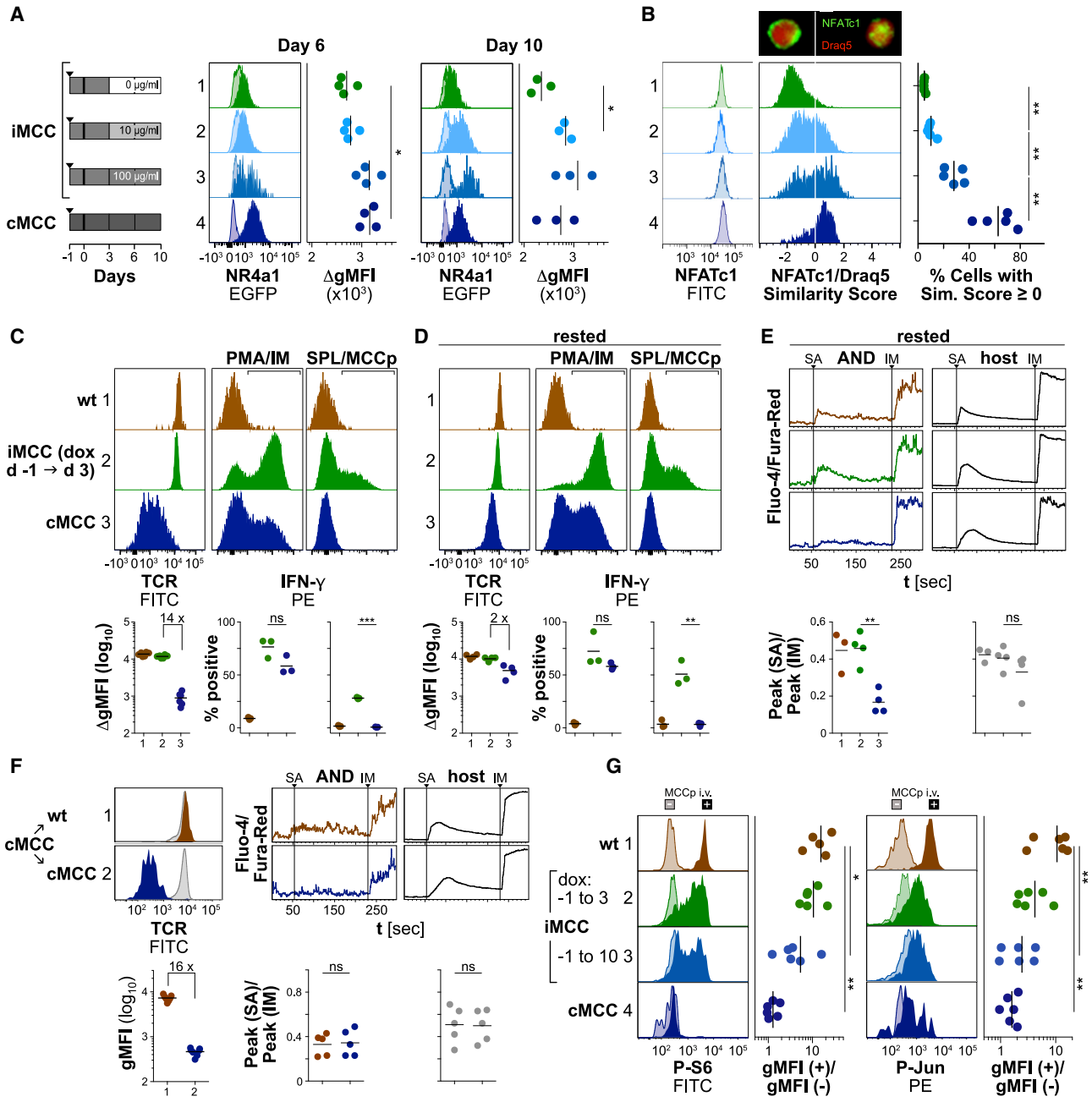

Figure 3. Chronic antigen presentation *in vivo* affects TCR signaling capacity

(A) Expression of the NR4a1-EGFP reporter in AND T cells transferred into four recipients and retrieved as indicated. Shaded histograms represent co-transferred reporter-negative AND T cells as specificity controls. Data are from four (day 6) and three (day 10) independent experiments.

(B) NFATc1 expression (left) and localization (right) in AND T cells among recipient splenocytes analyzed on day 10 pt. Data are compiled from five independent experiments.

(C) AND T cells retrieved from the indicated recipients were analyzed for TCR expression (left), or restimulated with PMA/IM (middle) or APCs and peptide (right panels). Data are compiled from three independent experiments with one to two animals per condition.

(D) AND T cells from recipients as described in (C), following an overnight culture in the absence of APCs. Data are from three independent experiments.

(E) Ca^{2+} flux of AND and host $CD4^+$ T cells from recipients as described in (C) following CD3/CD4-biotin crosslinking by adding streptavidin (SA) and IM. Data are compiled from four independent experiments.

(F) Ca^{2+} flux of AND and host $CD4^+$ T cells following a secondary transfer from cMCC into non-tg and cMCC recipients on day 10. On day 12 the cells were imaged as in (E). Data are from five independent experiments with one animal per condition.

(G) Signaling capacity of AND T cells retrieved from the indicated recipients. On day 10, animals were injected i.v. with PBS (shaded) or 100 µg $MCC_{93–103}$ peptide (filled histograms) and analyzed 1 h later. Data are compiled from six independent experiments with one animal per condition.

*$p < 0.05$, **$p < 0.005$, ***$p < 0.0005$ (unpaired Student's t test).

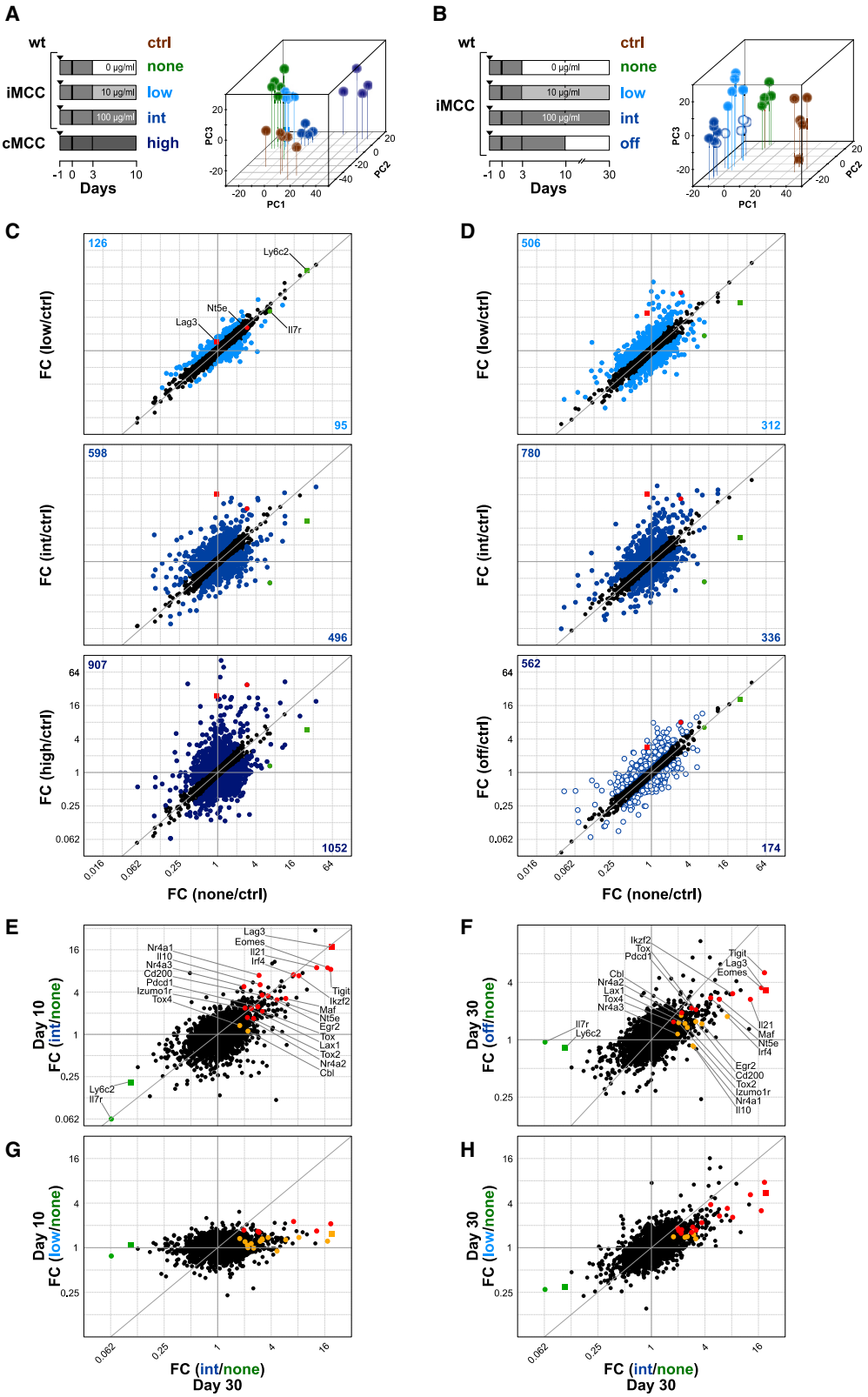

(legend on next page)

tested the phosphorylation of the AP-1 component Jun downstream of the MAPK cascade and found it decreased in correlation with the dose of persisting antigen (Figure 3G, right panels). These data indicated that TCR signaling pathways in $CD4^+$ T cells exposed chronically to antigen become differentially desensitized, or tuned, depending on antigen dose, with the Ca^{2+} pathway being more resistant to continuous input than the Akt/mTORC1 and MAPK pathways.

In summary, these data show two different mechanisms of exhaustion. We found that antigen is being recognized by $CD4^+$ T cells *in vivo* despite its chronicity, as far as the NR4a1 reporter and *ex vivo* NFAT translocation could indicate. When rechallenged following a resting period, however, cells exhausted at the high dose were, perhaps paradoxically, unable to flux Ca^{2+} and did not produce IFN-γ in response to strong TCR stimuli, pointing at an as yet unknown mechanism of TCR desensitization. Cells exhausted by intermediate-dose antigen did flux Ca^{2+} (Han et al., 2010) but showed reduced responses of the mTORC1 and MAPK pathways, suggesting an imbalance or asymmetry of TCR signaling pathways.

Dynamic regulation of gene expression in response to antigen persisting at different doses

We next examined AND T cells by sorting them from MCC-tg recipients on days 10 and 30 for microarray analysis. To assess the requirements of antigen persistence for the maintenance of exhaustion, MCC expression was turned off on day 10 in one group (T^{off}; see Figures 4A and 4B for schematics). Principal-component analyses (PCAs) of the day 10 data showed that cells exposed to no, intermediate, and high doses of antigen (T^{none}, T^{int}, and T^{high}, respectively) were easily separated by their expression signatures. The cells exposed to the low antigen dose (T^{low}), however, clustered with the T^{none} cells (Figure 4A), indicating that the low dose, clearly perceivable by naive T cells (Figure 1C), affects gene expression only minimally by day 10. This changes over time, because the signatures of cells exposed to the low antigen dose for an additional 20 days are positioned between T^{none} and T^{int} cells (Figure 4B). Interestingly, T^{off} cells partially split from the exhausted population, following a different trajectory (Figure 4B).

A more direct assessment of the early dosage effects is depicted in the fold change/fold change (FC/FC) comparisons of Figure 4C: low, intermediate, and high doses induce 126, 598, and 907 genes, respectively, more than 1.5-fold, many of which are not expressed in Tmem cells. Rather, memory markers *Il7r* and *Ly6c2* get suppressed with increasing antigen dose, with *Il7r* being the more sensitive gene. Genes associated with exhaustion and anergy, like *Lag3* and *Nt5e* (encoding CD73), however, are induced with increasing antigen dose (Figure 4C), indicating that antigen-driven $CD4^+$ T cell exhaustion consists of a dynamic response to antigen on day 10 already. By day 30, the low antigen dose had induced 506 genes (Figure 4D), about four times more than on day 10, indicating that $CD4^+$ T cells continuously accumulate low-level TCR signals and adjust their gene expression to the length of antigen presentation, reminiscent of the temporal summation of TCR signals shown in Figures 1B and 3A. For T^{int} cells, the data suggest that most of the chronic response to this antigen level was already set in place by day 10. This is confirmed in the direct comparison: genes associated with T cell anergy and exhaustion (among them indicated: *Cbl*, *Cd200*, *Egr2*, *Eomes*, *Il10*, *Il21*, *Irf4*, *Ikzf2* [encoding Helios], *Izumo1r* [encoding FR4], *Lag3*, *Lax1*, *Maf*, *Nr4a1-3*, *Nt5e*, *Pdcd1* [encoding PD-1], *Tigit*, *Tox*, *Tox2*, *Tox4*) crowd around the 1 = 1 diagonal in the T^{int} versus T^{none} comparisons of days 10 and 30 (Figure 4E). Many messages in T^{int} cells are actively maintained by antigen as they decline 20 days after turn-off (Figure 4F). Only 6 out of 21 anergy- and exhaustion-associated genes are induced by the low dose 10 days pt (Figure 4G), but by day 30, 16 of them are (Figure 4H), again demonstrating the possibility of signal summation over weeks for the development of anergy and exhaustion.

Similarities between antigen-exhausted $CD4^+$ T cells and naturally anergic and tumor-infiltrating ones

We then compared anergy signatures with the genes identified here by gene set enrichment analysis (GSEA). Unlike genes induced by costimulation-deficient APCs or IM, the signature induced by a constitutively active NFATc2 (NFAT1) variant is enriched in AND T^{int} and T^{high} cells on day 10 and in T^{low} and T^{int} cells on day 30 (Figure 5A). Genes expressed by $CD4^+$ TCR tg T cells following repeated peptide injections overlap in a very similar manner (Figure 5A). Genes expressed by $CD25^-CD45RB^{low}Lag3^+CD4^+$ T cells sorted from WT animals were significantly enriched in antigen-exhausted cells. We also sorted WT cells based on the anergy markers CD73 and FR4, which are expressed on a subset of $CD4^+$ T cells and $CD73^-FR4^-$ controls (Figure S2A). We found that genes expressed by such anergic cells are significantly enriched in antigen-exhausted cells, suggesting that this subset is constitutively triggered by antigen as well (Kalekar et al., 2016; Martinez et al., 2012; Figure 5A). Genes enriched in $FoxP3^-CD4^+$ T cells infiltrating B16 melanoma and MC38 adenocarcinoma tumors compared with splenocytes of the same phenotype are also preferentially found in antigen-exhausted and anergic $CD73^+FR4^+$ cells (Figure 5A), indicating their encounter of tolerogenic antigen in the tumor. These comparisons suggest that

Figure 4. Gene expression in antigen-exhausted AND T cells affected by dose and time

(A and B) PCA analyses of microarray data generated from AND T cells sorted from the indicated recipients on days 10 and 30.

(C and D) FC/FC plots of samples from AND T cells exhausted for 10 (C) or 30 days (D) by low (top panels), intermediate (middle panels), and high (bottom panels) levels of persisting antigen versus T^{none} cells, both compared with control cells. Two Tmem markers, *Il7r* (green circles) and *Ly6c2* (green squares), and two exhaustion markers, *Nt5e* (red circles) and *Lag3* (red squares), are indicated. Genes induced with an FC > 1.5 are colored, and their numbers are indicated in the panels.

(E–H) Gain and loss of genes associated with anergy and exhaustion depend on antigen encounter. Indicated genes fulfill the criteria FC > 1.5 and $p < 0.05$ regarding the intermediate (int)/none comparison on day 30 (all x axes). Genes in red fulfill these criteria regarding the comparisons indicated at the y axes, but yellow ones do not.

A

	CD4⁺ T cells	Source	Normalized Enrichment Score (NES) Day 10 low	Day 10 int	Day 10 high	Day 30 low	Day 30 int	Day 30 off	anergic
in vitro	OT-II (peptide, CD80/86/275-KO APCs)	Liu et al.,2019	1.6	2.0	-1.5	1.1	1.3	1.2	1.4
	D5 T cell clone (ionomycin, clusters 15-19)	Macián et al., 2002	0.9	1.6	1.8	1.0	1.2	1.3	1.6
	NFAT1-CA-RIT induced (adj p < 0.01)	Martinez et al., 2015	1.7	2.7	2.7	2.4	2.6	2.0	2.3
ex vivo	peptide-tolerized TCR-tg (FC≥ 2.0,p ≤ 0.01)	Bevington et al., 2020	1.1	2.3	2.6	1.9	2.6	2.3	2.5
	$CD25^{-}CD45RB^{low}LAG3^{+}$	Okamura et al., 2009	1.6	3.1	3.8	2.9	3.0	2.5	2.5
	$FR4^{+}CD73^{+}$(FC ≥2.0, p ≤ 0.01)	this study	1.8	3.1	3.1	2.7	2.8	2.1	
	$FoxP3^{-}$ B16 (FDR≤ 0.05)	Magnuson etal., 2018	1.2	1.6	2.1	2.0	1.9	2.2	2.6
	$FoxP3^{-}$ MC38 (FDR≤ 0.01)		1.1	1.9	2.6	2.2	2.1	1.7	2.8

B Day 10

Genes upregulated in one condition

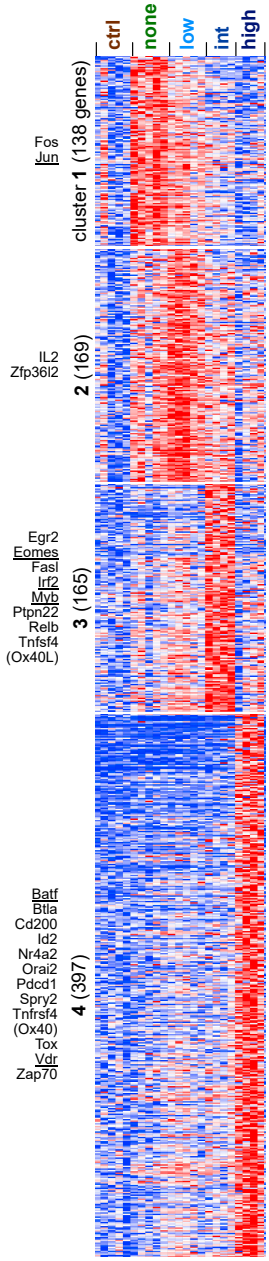

Genes upregulated in...

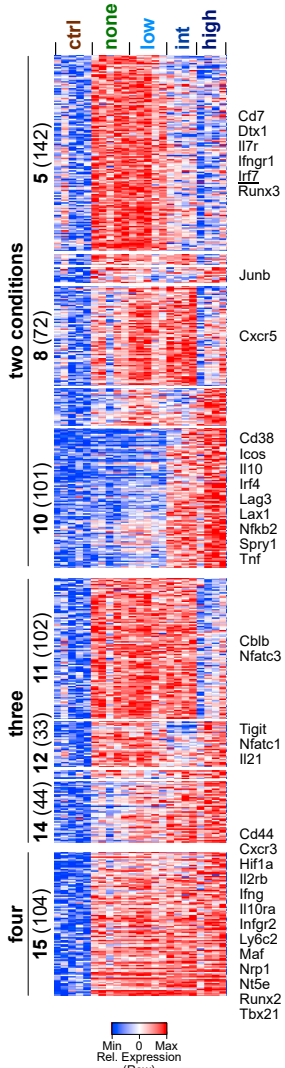

C Day 30

Genes upregulated in one condition

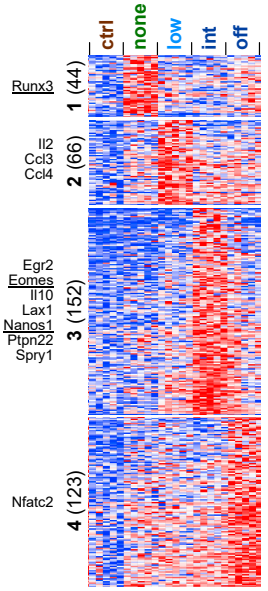

Genes upregulated in...

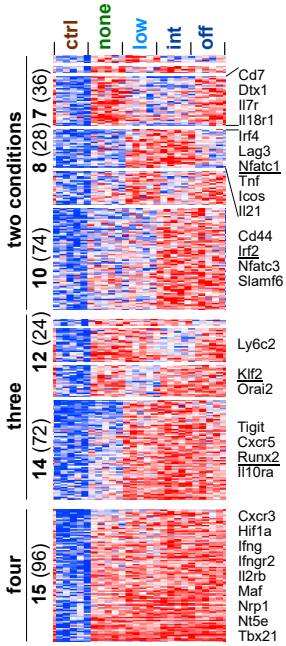

D

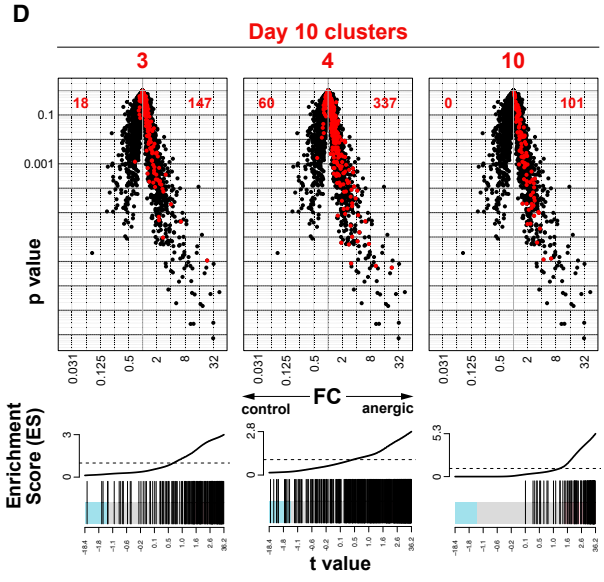

(legend on next page)

$CD4^+$ T cells of WT mice include an anergic subset similar to antigen-exhausted AND T cells. It remains to be determined which self-antigens or commensal antigens continuously trigger such anergic cells.

Varying precision of gene expression in response to antigen persisting at different doses

We next asked how precisely expression patterns are shaped by antigen persisting at different doses. We established a combinatorial matrix listing the 15 permutations of the four conditions, meeting the criteria FC >1.5 over controls and false discovery rate (FDR) <0.05 (Table S1). The resulting 15 clusters (cls) show that all degrees of dose dependencies can be found (Figures 5B and 5C). About half of the genes (57% and 50% on days 10 and 30, respectively) respond specifically to one dose only (cls 1–4); others respond less strictly under two or three conditions (5–14), while cl 15 is not affected by antigen changes after the activation phase at all (Figures 5B and 5C). Among the 1,518 genes found differentially expressed on day 10, several transcription factors can be identified, with those whose binding motifs are also enriched in the respective clusters underlined in Figures 5B and 5C. For example, *Batf*, *Id2*, *Nr4a2*, and *Tox*, associated with LCMV-driven exhaustion of $CD8^+$ T cells, are found on day 10 in cl 4 like *Pdcd1* and are thus driven only by antigen persisting at the highest level (Figure 5B). Others, like *Egr2* and *Eomes*, previously associated with anergy and exhaustion (Chappert and Schwartz, 2010; Paley et al., 2012), satisfy the clustering criteria in the T^{int} samples only (Figure 5B, cl 3), while *Irf4* (Man et al., 2017) appears in cl 10 and is thus expressed at both dosages. Cl 15 contains genes whose protein products are not affected by antigen persistence, like Cd44, common to Teff and Tmem cells. However, it also includes genes, like *Ly6c2* (Figure 2A) and *Ifng* (Figure 2B), whose proteins are affected by persisting antigen expression and are thus likely to be regulated post-transcriptionally.

The day 30 data show an overall "cooling down" with just 776 genes (51% of day 10) upregulated over controls (Figure 5B). The T^{off} samples differentiate between genes that depend on antigen persisting beyond day 10 (cl 3) or not (cl 10). In contrast, the memory markers *Il7r* and *Ly6c* are both upregulated when released from antigenic strain and are now found in cls 7 and 12, depending on their sensitivity to antigen persisting at the low dose.

The downregulated genes offer additional information on antigen-dependent gene expression (Figures S2B and S2C). Expression of *Izumo1r* (Kalekar et al., 2016; Martinez et al., 2012) requires antigen persistence at any dose, like *Egr1*, *Eomes*, *Irf4*, *Tox*, and *Pdcd1* (cl 1). *Foxo1*, encoding a transcription factor protecting $CD8^+$ T cells of anergy (Delpoux et al., 2018), is downregulated by the highest antigen concentration only (cl 4). *Cd69* is not expressed in any described here, excluding aspects of priming and the residential Tmem fate. The gene encoding the TCR adaptor protein LAT is downregulated in T^{high} cells only (Figure S2B, cl 4), which coincides with the TCR-proximal signaling block reported earlier (Figure 3) and was confirmed for the protein (Figure S2C). The fact that *Foxp3* is not induced in this system under the conditions tested and thus falls into cl 15 at both time points (Figures S2A and S2B) is confirmed by protein expression (Figure S2D). This is in agreement with the observation that AND $CD4^+$ T cells are unlikely to differentiate to the T regulatory cell (Treg) phenotype when stimulated by their cognate peptide (Szymczak-Workman et al., 2009; Yamashiro et al., 2002).

The cluster analysis also allows for better assessment in how far the exhausted phenotype of T^{int} cells is already set in place by day 10. The high levels of enrichment of genes upregulated in the day 10 samples in response to intermediate (cl 3), high (cl 4), both (cl 10), or any (cls 14, 15) dosages (Figure S3A) indicate that about half (147) of the genes specifically expressed on day 30 in exhausted T cells (299) have already been expressed on day 10 (Figure S3B).

In summary, these data illustrate, first, that gene expression of activated $CD4^+$ T cells is continuously and dynamically adjusted to antigen in the chronic phase, and second, that the sensitivity to antigen dose has a wide range of precision among the responding genes.

Signatures of antigen-exhausted cells compared with anergic and LCMV-exhausted cells

We next asked how antigen-exhausted cells compare with naturally occurring anergic T cells and sorted $CD4^+CD44^+CD73^+FR4^+$ and control $CD4^+CD44^+CD73^-FR4^-$ cells from non-tg B10.BR animals (Kalekar et al., 2016; Martinez et al., 2012). Figure S4A shows that such cells include $FoxP3^-$ and $FoxP3^+$ cells. Figures S4B and S4C show an increasing enrichment of genes with antigen dose. Interestingly, the concordance decreases by antigen removal, as indicated by the decreased enrichment score (ES; Figure S4B, right panel). We also found that genes expressed at intermediate, high, or both of these doses (cls 3, 4, and 10) are highly enriched in anergic cells (Figure 5D), like genes not

Figure 5. Similarities of antigen-exhausted to anergic and tumor-infiltrating $CD4^+$ T cells and varying precision of gene expression in response to antigen persisting at different doses

(A) Enrichment of signature genes expressed by anergic and tumor-infiltrating $CD4^+$ T cells, in day 10 and day 30 populations compared with naive controls. Last column: $CD4^+CD44^+CD73^+FR4^+$ anergic cells sorted as in Figure S2A. For all comparisons with Normalized Enrichment Score (NES) $\geq$ 1.6: FDR $\leq$ 0.002. In vitro data from Liu et al., 2019; Macián et al., 2002; and Martinez et al., 2015. Ex vivo data from Bevington et al., 2020; Okamura et al., 2009; Magnuson et al., 2018; and this study.

(B and C) Comparisons of gene expression in all conditions on days 10 (B) and 30 (C). Differential expression defined by FC > 1.5 and FDR < 0.05 was determined by comparing each treatment condition with the corresponding control. Genes were grouped in heatmaps according to the pattern of upregulation across all conditions according to Table S1, which also lists minimal and maximal relative expression values for each cluster. Transcription factors whose binding sites are also enriched are underlined.

(D) Differences between WT control ($CD73^-FR4^-$) and anergic ($CD73^+FR4^+$) $CD44^+CD4^+$ T cells sorted as in Figure S2A. Highlighted in red are the genes of the indicated clusters in (A). Numbers indicate the genes with FC < 1 (left) and FC > 1 (right).

See also Figures S2–S7.

affected by antigen persistence (cl 15), although there is no enrichment of genes in the T^{none}-associated cl 1 (Figure S5A). Out of all the genes enriched in anergic cells (545), about half of them (271) are also expressed in antigen-exhausted cells on day 10 or 30 (Figure S5B). This finding illustrates the antigen-dependent nature of gene expression in naturally anergic T cells. At the same time, this group of cells may also consist of cells of other lineages or fates, like Treg precursors, Tregs (Kalekar et al., 2016), or cells controlled by them (Martinez et al., 2012; Tuncel et al., 2019).

Because the LCMV cl13 model of T cell exhaustion includes dramatic aspects of chronic inflammation and cachexia (Baazim et al., 2019; Lercher et al., 2019; Snell et al., 2017), we asked what part of cl13-associated genes is induced by persisting antigen (Crawford et al., 2014). We first noticed that they correlated best with genes expressed by T^{high} cells (Figure S6A), confirmed by projections of exhaustion-associated clusters of day 10 and 30 data (Figures S6B and S6C). When we looked at genes expressed in $CD4^+$ T cells responding to chronic versus acute LCMV variants (113 and 90 genes on days 15 and 30, respectively), but not in any of the three antigen dosages analyzed here (45 and 77 genes), we found an enrichment of signatures associated with innate, antiviral, and IFN responses (Tables S2 and S3). These data highlight the fact that a good part of genes enriched in $CD4^+$ T cells of chronic versus acute LCMV comparisons, 40% and 86% on days 15 and 30, respectively, are not found in antigen-exhausted Th cells and are thus likely to be driven by innate aspects of antiviral immune responses rather than antigen persistence.

A Gene Ontology (GO) term analysis of the clusters showed an enrichment of genes affecting signal transduction on the transcriptional level in several clusters, with second messenger signaling, phosphorylation, phospholipase C, and the MAPK pathway affected in T^{int} and T^{high} cells (cl 10; Figure S7), and PIP_2- and nuclear factor κB (NF-κB)-mediated signaling being downregulated in T^{high} cells (cl 4). These data suggest a desensitization of TCR signaling is partially due to transcriptional adjustment to persisting antigen.

Antigen-induced anergy marker expression remains antigen-dependent and reversible

The gene expression data suggested that antigen persisting at intermediate and high doses between days 5 and 10 elicited two distinct phenotypes. We indeed found inhibitory receptors PD-1, LAG3, TIGIT, and CD200, but also costimulatory receptor Ox40 (CD134) and IL-18R expressed in a dose-dependent manner (Figure 6A). This also applied to the transcription factors Maf and Tox, with Tox being more sensitive to antigen (Figure 6B), confirming their early role in exhaustion (Giordano et al., 2015; Mann and Kaech, 2019).

CD73 and FR4 are markers of anergic $CD4^+$ T cells in models of arthritis and allogenic pregnancy (Kalekar et al., 2016; Martinez et al., 2012). The allocation of their respective genes, *Nt5e* and *Izumo1r*, in cl 15 (up, Figures 5B and 5C) and cl 1 (down, Figures S2A and S2B), respectively, would not account for being associated with antigen-induced exhaustion and indicate post-transcriptional regulation of CD73. Out of the recipients' $CD4^+$ T cells, 19.5% ± 6.9% fell into the $CD73^+FR4^+$ gate, while the AND T cells in it increased from 3.0% ± 3.0% (Figure 6C, condition 2, T^{none}) to 83.4% ± 6.9% (condition 5, T^{high}) in a dose-dependent manner. These data indicated, first, that an increasing antigen load between days 5 and 10 correlates with CD73 and FR4 expression, and second, that the anergic cells do not compete with endogenous anergic cells for a niche or a limiting resource, because their numbers did not change (Figure 6C).

We then compared CD73 and FR4 expression after antigen presentation was continued at the intermediate level in the iMCC recipients or turned off on day 10 (Figure 6D, conditions 1–3). In addition, we performed secondary transfers of AND T^{high} cells to cMCC animals or non-tg hosts (Figure 6D, conditions 4 and 5). In both setups, the AND cells found on day 21 in conditions 3 and 5 had mostly lost the expression of the markers, indicating that their expression depended on antigen persistence. These data are in agreement with the reversible surface phenotype, functionalities, and gene expression shown in Figures 1, 4, and 5. They also recall results on LCMV- and liver/cancer-exhausted $CD8^+$ T cells whose phenotype remained flexible for around 2 weeks of chronic stimulation (Angelosanto et al., 2012; Philip et al., 2017).

Antigen-exhausted $CD4^+$ T cells lose their ability to deliver help to B cells over time

It has been discussed whether $CD4^+$ Th1 cells are merely dysfunctional in chronic infections (Brooks et al., 2006) or differentiate into T follicular helper (Tfh) cells (Crawford et al., 2014; Fahey et al., 2011) or another cell type able to deliver help to $CD8^+$ T cells via IL-21 (Vella et al., 2017). We noticed that several mRNAs associated with T-B cell interaction and Maf, Tox, CXCR5, and ICOS proteins were affected by antigen persistence (Kroenke et al., 2012; Xu et al., 2019; Figures 6B and 7A). We thus assayed the capacity of T^{int} and T^{none} AND cells to deliver help to adoptively transferred CFSE-labeled cMCC B cells that expressed an Ig specific for the model antigen hen egg lysozyme (HEL). Such B cells proliferated in response to MCC-specific T cells only if HEL and dox are given to activate the respective B and T cell antigen receptors simultaneously (Figure 7B, conditions 1–4). T^{int} cells exhausted for 10 days were only partially able to support the B cells' proliferation (condition 5), while the cells exhausted for 30 days could not (condition 6). This functional exhaustion over time correlates with the impaired or absent CD154 expression upon strong PMA/IM restimulation on days 10 (Figure 2C) and 30 (Figure 1G), respectively, which is essential for any productive interaction between T and B cells (Laman et al., 2017).

DISCUSSION

Peripheral deletion of specific T cells has been observed in tolerance mediated by bone marrow chimerism, in responses to incompletely activated APCs, in chronic infections like HCV, and among T cells specific for certain LCMV cl13 epitopes (Bonifaz et al., 2004; ElTanbouly and Noelle, 2020; Schulze zur Wiesch et al., 2012; Wherry et al., 2003; Zuber and Sykes, 2017). TCR downregulation has been described as a mechanism to regulate antigen-specific reactivity to high levels of bacterial,

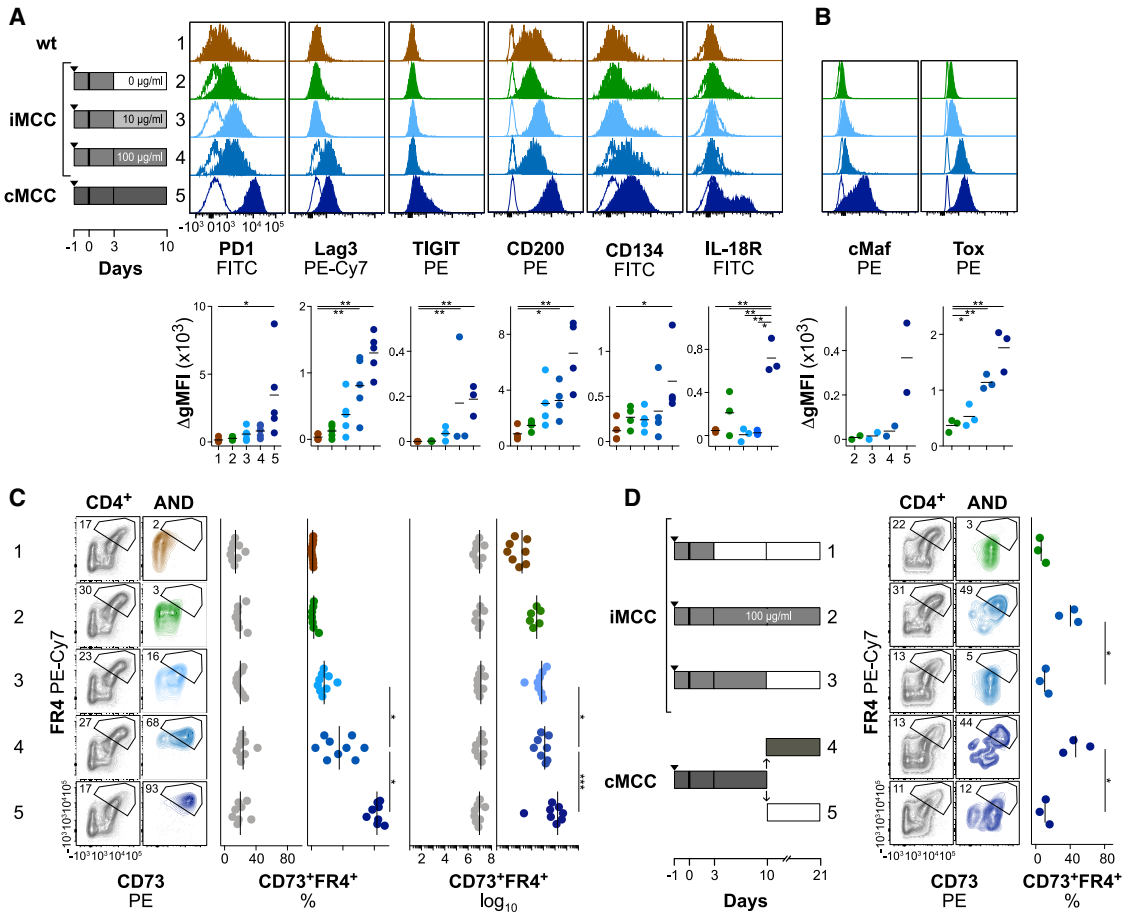

Figure 6. Antigen dependence of exhaustion and anergy marker expression

(A and B) Expression of surface markers (A) and transcription factors (B) by AND T cells from the recipients depicted on the left. Data are pooled from two to five independent experiments with n = 1 recipient per condition; each symbol represents one recipient.

(C) Expression of the anergy markers CD73 and FR4 by host $CD4^+$ (left, gray) and AND T cells from the recipients shown in (A) on day 10 pt (colored, right). Percentages (left) and cell numbers (right) of $CD73^+FR4^+$ T cells among endogenous $CD4^+$ (left, gray) and adoptively transferred AND T cells are shown. Data are compiled from six independent experiments with n = 1–3 recipients per condition.

(D) CD73 and FR4 expression by endogenous and AND T cells of the indicated recipients. Data are from three experiments with n = 1 recipient per condition. *p < 0.05, **p < 0.005, ***p < 0.0005 (unpaired Student's t test).

natural, and neo-self-antigens (Ferber et al., 1994; Gallegos et al., 2016; Holst et al., 2008; Reeves et al., 2017; Teague et al., 2008). At the highest antigen dose studied here, the cells were continuously stimulated via the Ca^{2+} pathway despite receptor internalization. Such signals may be initiated by the few TCR molecules at the surface or from internalized ones in endocytic compartments, perhaps triggered by E^k/MCC complexes trogocytosed with them (Labrecque et al., 2001; Reed and Wetzel, 2019; Saveanu et al., 2019). However, responsiveness to acute TCR crosslinking was defunct and could not be recovered by TCR re-expression in the absence of antigen. This finding points at an as yet unidentified proximal signaling component that is required to respond to discontinuous TCR signals but remains dysfunctional in T cells chronically exposed to high antigen levels (Chiodetti et al., 2006; Teague et al., 2008). The recruitment of early signaling components like LAT from intracellular membrane pools to the TCR is a critical step of signal initiation and also found dampened in early anergy models (Courtney et al., 2018; Hundt et al., 2006; Saveanu et al., 2019). Interestingly, its downregulation coincided with the increased expression of its regulator Lax1, which has also been identified in LCMV-exhausted $CD8^+$ T cells (Crawford et al., 2014; Hudson et al., 2019; Zhu et al., 2005). Another possibility is that epigenetic modifications affect the expression of TCR signaling components irreversibly.

The accumulation of weak signals over a period of weeks for exhaustion came as a surprise. The integration of TCR signals at low antigen levels or over experimental interruptions has been described for T cell priming (Clark et al., 2011; Faroudi et al., 2003; Henrickson et al., 2008) and has suggested a persisting signaling intermediate (Moreau and Bousso, 2014; Rachmilewitz and Lanzavecchia, 2002). The dynamic adjustment to chronic antigen presentation leading to partial impairment over time may explain the maintenance of functional responsiveness

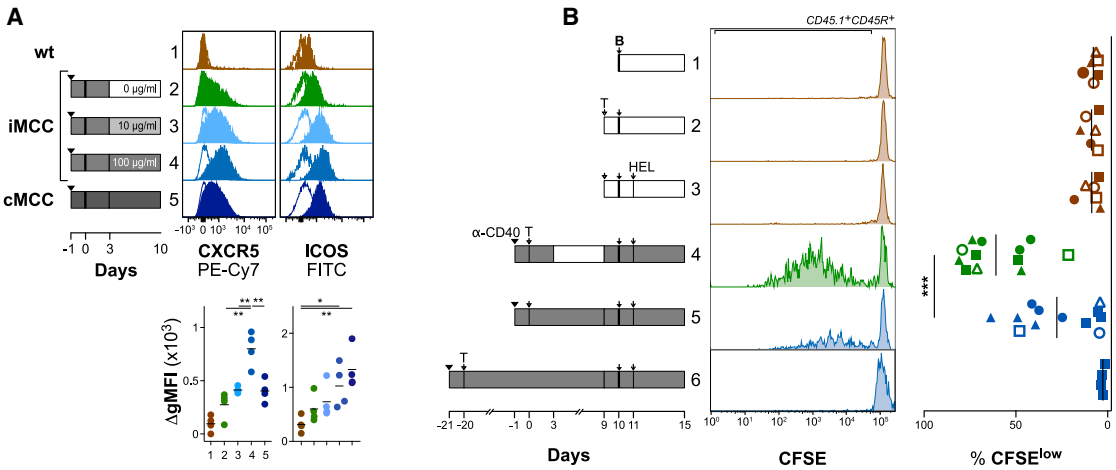

Figure 7. Chronically antigen-exhausted CD4⁺ T cells lose the ability to transmit help to B cells

(A) CXCR5 and ICOS expression on AND T cells exposed to antigen as shown.

(B) Proliferation profiles of allogenically marked B cells carrying the anti-HEL-Ig and the cMCC transgene exposed to AND T cells following the indicated treatments. Data are pooled from six independent experiments represented by different symbols.

*p < 0.05, **p < 0.005, ***p < 0.0005 (unpaired Student's t test).

to latent infections like EBV and CMV in men and MHV68 and *T. cruzi* in mice. These pathogens do not elicit exhausted but more complex T cell phenotypes with functionalities sufficient to rein in the respective microbes (Hu et al., 2015; Pack et al., 2018). Accordingly, focusing antigen presentation to DC in a chronic LCMV infection also reduced the level of T cell exhaustion (Richter et al., 2012).

In germinal centers, CD4⁺ T cells are exposed to antigen for a long time. Because their functionality is necessary for the development of high-affinity antibodies, they may be able to buffer the development of dysfunctionalities. The correlation between viremia and Tfh signatures in HIV patients and the successful application of slow-release protein immunization for prolonged germinal center responses confirm this notion (Cirelli et al., 2019; Morou et al., 2019). The appearance of broadly neutralizing antibodies against HIV-env 2–4 years after infection suggests the stability of Tfh functionality despite protracted env exposure (Borrow and Moody, 2017). In the iMCC system, we observed that the T cells become increasingly unable to induce B cell proliferation over time when stimulated by DC only. CD40 and CD154 transmit signals necessary for productive T-B cell interactions (Laman et al., 2017), but CD154 expression upon re-stimulation is impaired or absent on T^{int} cells. Because Tfh differentiation occurs via a DC-dependent step toward pre-Tfh cells and a B cell-dependent step (Baumjohann et al., 2011, 2013; Goenka et al., 2011), it is tempting to speculate that the anergic/exhausted T cells described here share features with pre-Tfh cells. Thus, our findings argue for a dynamic adaptation to chronic antigen challenge similar to naive CD4⁺ T cell TCR tuning by self-peptide/MHC complexes (Grossman and Paul, 2015; Myers et al., 2017; Zinzow-Kramer et al., 2019), rather than for a fixed fate or lineage of exhausted T cells as it has been proposed for CD8⁺ ones (McLane et al., 2019). This is in agreement with data on chronic LCMV infections where germinal centers develop slowly and their B cells hypermutate and secrete neutralizing antibodies, very likely controlled by CD4⁺ Th cells (Fallet et al., 2020).

The T^{int} cells' TCRs were not internalized and perceived antigen, but their mTORC1 and MAPK pathways became desensitized to antigenic challenge with the Ca^{2+} response not affected (Han et al., 2010). This continuous asymmetrical signaling induced a signature, including anergy and exhaustion markers, which were only slowly downregulated following antigen removal, suggesting epigenetic regulation (Philip et al., 2017). The desensitization of the MAPK pathway harks back to findings on anergic cells and holds therapeutic promise. TCR signal transduction via the MAPK and the phosphatidylinositol 3-kinase (PI3K)/Akt/mTORC1 pathways is hampered in anergy (Chappert and Schwartz, 2010; Chiodetti et al., 2006). An experimental mimic of it was the asymmetrical stimulation of T cells with low levels of Ca^{2+} ionophores, leading to the first molecular definitions of anergy (Hundt et al., 2006; Macián et al., 2002). A constitutively active NFATc2 variant unable to interact with AP-1 can also replace asymmetrical TCR signals and induce expression signatures resembling anergic and exhausted cells (Martinez et al., 2015). The expression of the exhaustion-associated transcription factor Tox can be triggered in naive CD8⁺ T cells by Ca^{2+} ionophore treatment alone, suggesting asymmetrical signaling in LCMV-exhausted T cells as well (Mann and Kaech, 2019). Insufficient AP-1 expression can also contribute to asymmetrical signaling (Mondino et al., 1996): Tmem cells increased the expression of Fos and Jun, while persisting antigen tuned it down (Figure 5B, cl 1). This was recently used by overexpressing the AP-1 component c-Jun to reconstitute a CAR T cell product prone to exhaustion (Lynn et al., 2019). Another possibility of recovering AP-1 activity was achieved by pharmaceutical inhibition of the MAPK pathway that resuscitated T cell activity in tumor models by temporarily releasing cells from MAPK-mediated exhaustive stress (Ebert et al., 2016; Verma et al., 2021).

The transcriptional data display the ripples persisting antigen makes through the genome. Low-dose antigen presentation takes weeks to induce exhaustion-associated genes, while the exhaustion-associated signature of T^{int} cells is already in place by day 10 but pliable as it subsides over weeks following antigen withdrawal. This response is much slower than in the expansion phase, where overall gene expression is massively affected by antigen withdrawal within days (Rabenstein et al., 2014). A "point of no return" between days 7 and 14 has been described for exhausted $CD8^+$ T cells in a liver/cancer model because of substantial epigenetic changes (Philip et al., 2017). Although the difference may lie in the T cell subset or the tolerogenic liver microenvironment investigated, it remains to be determined whether the pliability of $CD4^+$ T cells is maintained at later time points.

We hope our data on the transcriptional signatures of both naturally anergic and cells experimentally exhausted by graded antigen presentation will help to integrate future findings and supply investigators of TCR-mediated T cell tolerance with an opportunity to explore molecular possibilities of intervention and therapy in autoimmunity and chronic diseases.

The idea that immune cells mainly perceive discontinuous changes has been proposed to unify receptor logics of innate and adaptive immune systems. According to that proposal, the immune response is a change detection system where slow changes would lead to tolerance (Pradeu and Vivier, 2016). We have shown here that $CD4^+$ T cells responding to chronic antigen adapt their responsiveness dynamically, which is consistent with this notion.

STAR★METHODS

Detailed methods are provided in the online version of this paper and include the following:

- KEY RESOURCES TABLE
- RESOURCE AVAILABILITY
  - Lead contact
  - Materials availability
  - Data and code availability
- EXPERIMENTAL MODEL AND SUBJECT DETAILS
  - Mice
- METHOD DETAILS
  - Animal Treatments and Adoptive Transfers
  - CTV Labeling
  - Flow Cytometry: Standard Stainings
  - Cytokines
  - Phosphorylated Proteins
  - NFAT Localization
  - Ca^{2+} Responsiveness
  - Cell Sorting
  - Quantitative RT-PCR: Assessment of Transgene Expression
  - Transcriptome Analysis: RNA Isolation
  - Expression Profiling
- QUANTIFICATION AND STATISTICAL ANALYSIS
  - Cytometry Data Analysis
  - Transcriptomic Data Analysis

SUPPLEMENTAL INFORMATION

Supplemental Information can be found online at https://doi.org/10.1016/j.celrep.2021.108748.

ACKNOWLEDGMENTS

The authors thank R. Brink for providing SW_{HEL} mice and C. Terhorst and M. Turner for providing $SAP^{o/o}$ animals; M. Bamberger (Helmholtz) and A. Kollar and S. Pentz (Immunology) for expert technical assistance; W. Nakagawa for help with initial experiments; J. Klein for expert assistance with the ImageStream cytometer at the Core Facility Flow Cytometry; L. Henckel and M. Schiemann (Cytometry Technical University Munich) and P. Khosravani (Core Facility Flow Cytometry at the Biomedical Center) for cell sorting; and A. Bol, B. Popper, and colleagues for expert animal husbandry. This work benefitted from data assembled by the ImmGen consortium. This work was supported by CRC 1054-B07 (R.O.) and 1054-B03 (T.B.) of the German Research Council (Deutsche Forschungsgemeinschaft) and the Helmholtz Alliance "Aging and Metabolic Programming, AMPro" (J.B.).

AUTHOR CONTRIBUTIONS

Conceptualization, A.T. and R.O.; investigation, A.T., P.K., S.-H.W., S.P., B.L.; formal analysis, B.A., M.I., T.S.; data curation, T.S.; writing – original draft, R.O.; writing – review & editing, A.T., P.K., S.-H.W., B.A., J.K., N.N., R.O.; funding acquisition, J.B., T.B., R.O.; resources, N.N.; Supervision, J.B., T.S., R.O.

DECLARATION OF INTERESTS

The authors declare no competing interests.

Received: February 24, 2020
Revised: September 21, 2020
Accepted: January 19, 2021
Published: February 9, 2021

REFERENCES

Alspach, E., Lussier, D.M., Miceli, A.P., Kizhvatov, I., DuPage, M., Luoma, A.M., Meng, W., Lichti, C.F., Esaulova, E., Vomund, A.N., et al. (2019). MHC-II neoantigens shape tumour immunity and response to immunotherapy. Nature *574*, 696–701.

Angelosanto, J.M., Blackburn, S.D., Crawford, A., and Wherry, E.J. (2012). Progressive loss of memory T cell potential and commitment to exhaustion during chronic viral infection. J. Virol. *86*, 8161–8170.

Aubert, R.D., Kamphorst, A.O., Sarkar, S., Vezys, V., Ha, S.J., Barber, D.L., Ye, L., Sharpe, A.H., Freeman, G.J., and Ahmed, R. (2011). Antigen-specific CD4 T-cell help rescues exhausted CD8 T cells during chronic viral infection. Proc. Natl. Acad. Sci. USA *108*, 21182–21187.

Baazim, H., Schweiger, M., Moschinger, M., Xu, H., Scherer, T., Popa, A., Gallage, S., Ali, A., Khamina, K., Kosack, L., et al. (2019). $CD8^+$ T cells induce cachexia during chronic viral infection. Nat. Immunol. *20*, 701–710.

Baumjohann, D., Okada, T., and Ansel, K.M. (2011). Distinct waves of BCL6 expression during T follicular helper cell development. J. Immunol. *187*, 2089–2092.

Baumjohann, D., Preite, S., Reboldi, A., Ronchi, F., Ansel, K.M., Lanzavecchia, A., and Sallusto, F. (2013). Persistent antigen and germinal center B cells sustain T follicular helper cell responses and phenotype. Immunity *38*, 596–605.

Bevington, S.L., Ng, S.T.H., Britton, G.J., Keane, P., Wraith, D.C., and Cockerill, P.N. (2020). Chromatin priming renders T cell tolerance-associated genes sensitive to activation below the signaling threshold for immune response genes. Cell Rep. *31*, 107748.

Bonifaz, L.C., Bonnyay, D.P., Charalambous, A., Darguste, D.I., Fujii, S., Soares, H., Brimnes, M.K., Moltedo, B., Moran, T.M., and Steinman, R.M.

(2004). In vivo targeting of antigens to maturing dendritic cells via the DEC-205 receptor improves T cell vaccination. J. Exp. Med. *199*, 815–824.

Borrow, P., and Moody, M.A. (2017). Immunologic characteristics of HIV-infected individuals who make broadly neutralizing antibodies. Immunol. Rev. *275*, 62–78.

Borst, J., Ahrends, T., Bąbała, N., Melief, C.J.M., and Kastenmüller, W. (2018). $CD4^+$ T cell help in cancer immunology and immunotherapy. Nat. Rev. Immunol. *18*, 635–647.

Brooks, D.G., Teyton, L., Oldstone, M.B., and McGavern, D.B. (2005). Intrinsic functional dysregulation of CD4 T cells occurs rapidly following persistent viral infection. J. Virol. *79*, 10514–10527.

Brooks, D.G., McGavern, D.B., and Oldstone, M.B. (2006). Reprogramming of antiviral T cells prevents inactivation and restores T cell activity during persistent viral infection. J. Clin. Invest. *116*, 1675–1685.

Celli, S., Garcia, Z., and Bousso, P. (2005). CD4 T cells integrate signals delivered during successive DC encounters in vivo. J. Exp. Med. *202*, 1271–1278.

Chappert, P., and Schwartz, R.H. (2010). Induction of T cell anergy: integration of environmental cues and infectious tolerance. Curr. Opin. Immunol. *22*, 552–559.

Chiodetti, L., Choi, S., Barber, D.L., and Schwartz, R.H. (2006). Adaptive tolerance and clonal anergy are distinct biochemical states. J. Immunol. *176*, 2279–2291.

Cirelli, K.M., Carnathan, D.G., Nogal, B., Martin, J.T., Rodriguez, O.L., Upadhyay, A.A., Enemuo, C.A., Gebru, E.H., Choe, Y., Viviano, F., et al. (2019). Slow delivery immunization enhances HIV neutralizing antibody and germinal center responses via modulation of immunodominance. Cell *177*, 1153–1171.e28.

Clark, C.E., Hasan, M., and Bousso, P. (2011). A role for the immediate early gene product c-fos in imprinting T cells with short-term memory for signal summation. PLoS ONE *6*, e18916.

Cornberg, M., Kenney, L.L., Chen, A.T., Waggoner, S.N., Kim, S.K., Dienes, H.P., Welsh, R.M., and Selin, L.K. (2013). Clonal exhaustion as a mechanism to protect against severe immunopathology and death from an overwhelming CD8 T cell response. Front. Immunol. *4*, 475.

Courtney, A.H., Lo, W.L., and Weiss, A. (2018). TCR signaling: mechanisms of initiation and propagation. Trends Biochem. Sci. *43*, 108–123.

Crawford, A., Angelosanto, J.M., Kao, C., Doering, T.A., Odorizzi, P.M., Barnett, B.E., and Wherry, E.J. (2014). Molecular and transcriptional basis of $CD4^+$ T cell dysfunction during chronic infection. Immunity *40*, 289–302.

Delpoux, A., Michelini, R.H., Verma, S., Lai, C.Y., Omilusik, K.D., Utzschneider, D.T., Redwood, A.J., Goldrath, A.W., Benedict, C.A., and Hedrick, S.M. (2018). Continuous activity of Foxo1 is required to prevent anergy and maintain the memory state of $CD8^+$ T cells. J. Exp. Med. *215*, 575–594.

Ebert, P.J.R., Cheung, J., Yang, Y., McNamara, E., Hong, R., Moskalenko, M., Gould, S.E., Maecker, H., Irving, B.A., Kim, J.M., et al. (2016). MAP kinase inhibition promotes T cell and anti-tumor activity in combination with PD-L1 checkpoint blockade. Immunity *44*, 609–621.

ElTanbouly, M.A., and Noelle, R.J. (2020). Rethinking peripheral T cell tolerance: checkpoints across a T cell's journey. Nat. Rev. Immunol. Published online October 19, 2020. https://doi.org/10.1038/s41577-020-00454-2.

Fahey, L.M., Wilson, E.B., Elsaesser, H., Fistonich, C.D., McGavern, D.B., and Brooks, D.G. (2011). Viral persistence redirects CD4 T cell differentiation toward T follicular helper cells. J. Exp. Med. *208*, 987–999.

Fallet, B., Hao, Y., Florova, M., Cornille, K., de Los Aires, A.V., Girelli Zubani, G., Ertuna, Y.I., Greiff, V., Menzel, U., Hammad, K., et al. (2020). Chronic viral infection promotes efficient germinal center B cell responses. Cell Rep. *30*, 1013–1026.e7.

Faroudi, M., Zaru, R., Paulet, P., Müller, S., and Valitutti, S. (2003). Cutting edge: T lymphocyte activation by repeated immunological synapse formation and intermittent signaling. J. Immunol. *171*, 1128–1132.

Fazilleau, N., McHeyzer-Williams, L.J., Rosen, H., and McHeyzer-Williams, M.G. (2009). The function of follicular helper T cells is regulated by the strength of T cell antigen receptor binding. Nat. Immunol. *10*, 375–384.

Ferber, I., Schönrich, G., Schenkel, J., Mellor, A.L., Hämmerling, G.J., and Arnold, B. (1994). Levels of peripheral T cell tolerance induced by different doses of tolerogen. Science *263*, 674–676.

Ferris, S.T., Durai, V., Wu, R., Theisen, D.J., Ward, J.P., Bern, M.D., Davidson, J.T., 4th, Bagadia, P., Liu, T., Briseño, C.G., et al. (2020). cDC1 prime and are licensed by $CD4^+$ T cells to induce anti-tumour immunity. Nature *584*, 624–629.

Frebel, H., Richter, K., and Oxenius, A. (2010). How chronic viral infections impact on antigen-specific T-cell responses. Eur. J. Immunol. *40*, 654–663.

Fuller, M.J., and Zajac, A.J. (2003). Ablation of CD8 and CD4 T cell responses by high viral loads. J. Immunol. *170*, 477–486.

Gallegos, A.M., Xiong, H., Leiner, I.M., Sušac, B., Glickman, M.S., Pamer, E.G., and van Heijst, J.W. (2016). Control of T cell antigen reactivity via programmed TCR downregulation. Nat. Immunol. *17*, 379–386.

Giordano, M., Henin, C., Maurizio, J., Imbratta, C., Bourdely, P., Buferne, M., Baitsch, L., Vanhille, L., Sieweke, M.H., Speiser, D.E., et al. (2015). Molecular profiling of CD8 T cells in autochthonous melanoma identifies *Maf* as driver of exhaustion. EMBO J. *34*, 2042–2058.

Goenka, R., Barnett, L.G., Silver, J.S., O'Neill, P.J., Hunter, C.A., Cancro, M.P., and Laufer, T.M. (2011). Dendritic cell-restricted antigen presentation initiates the follicular helper T cell program but cannot complete ultimate effector differentiation. J. Immunol. *187*, 1091–1095.

Greczmiel, U., Kräutler, N.J., Pedrioli, A., Bartsch, I., Agnellini, P., Bedenikovic, G., Harker, J., Richter, K., and Oxenius, A. (2017). Sustained T follicular helper cell response is essential for control of chronic viral infection. Sci. Immunol. *2*, eaam8686.

Grossman, Z., and Paul, W.E. (2015). Dynamic tuning of lymphocytes: physiological basis, mechanisms, and function. Annu. Rev. Immunol. *33*, 677–713.

Haabeth, O.A., Tveita, A.A., Fauskanger, M., Schjesvold, F., Lorvik, K.B., Hofgaard, P.O., Omholt, H., Munthe, L.A., Dembic, Z., Corthay, A., and Bogen, B. (2014). How do $CD4^+$ T cells detect and eliminate tumor cells that either lack or express MHC class II molecules? Front. Immunol. *5*, 174.

Han, S., Asoyan, A., Rabenstein, H., Nakano, N., and Obst, R. (2010). Role of antigen persistence and dose for $CD4^+$ T-cell exhaustion and recovery. Proc. Natl. Acad. Sci. USA *107*, 20453–20458.

Harker, J.A., Lewis, G.M., Mack, L., and Zuniga, E.I. (2011). Late interleukin-6 escalates T follicular helper cell responses and controls a chronic viral infection. Science *334*, 825–829.

Hashimoto, M., Kamphorst, A.O., Im, S.J., Kissick, H.T., Pillai, R.N., Ramalingam, S.S., Araki, K., and Ahmed, R. (2018). CD8 T cell exhaustion in chronic infection and cancer: Opportunities for interventions. Annu. Rev. Med. *69*, 301–318.

Hataye, J., Moon, J.J., Khoruts, A., Reilly, C., and Jenkins, M.K. (2006). Naive and memory $CD4^+$ T cell survival controlled by clonal abundance. Science *312*, 114–116.

Henrickson, S.E., Mempel, T.R., Mazo, I.B., Liu, B., Artyomov, M.N., Zheng, H., Peixoto, A., Flynn, M.P., Senman, B., Junt, T., et al. (2008). T cell sensing of antigen dose governs interactive behavior with dendritic cells and sets a threshold for T cell activation. Nat. Immunol. *9*, 282–291.

Hogan, P.G., Chen, L., Nardone, J., and Rao, A. (2003). Transcriptional regulation by calcium, calcineurin, and NFAT. Genes Dev. *17*, 2205–2232.

Holst, J., Wang, H., Eder, K.D., Workman, C.J., Boyd, K.L., Baquet, Z., Singh, H., Forbes, K., Chruscinski, A., Smeyne, R., et al. (2008). Scalable signaling mediated by T cell antigen receptor-CD3 ITAMs ensures effective negative selection and prevents autoimmunity. Nat. Immunol. *9*, 658–666.

Hu, Z., Blackman, M.A., Kaye, K.M., and Usherwood, E.J. (2015). Functional heterogeneity in the $CD4^+$ T cell response to murine γ-herpesvirus 68. J. Immunol. *194*, 2746–2756.

Hudson, W.H., Gensheimer, J., Hashimoto, M., Wieland, A., Valanparambil, R.M., Li, P., Lin, J.X., Konieczny, B.T., Im, S.J., Freeman, G.J., et al. (2019). Proliferating transitory T cells with an effector-like transcriptional signature emerge from $PD\text{-}1^+$ stem-like $CD8^+$ T cells during chronic infection. Immunity *51*, 1043–1058.e4.

Hundt, M., Tabata, H., Jeon, M.S., Hayashi, K., Tanaka, Y., Krishna, R., De Giorgio, L., Liu, Y.C., Fukata, M., and Altman, A. (2006). Impaired activation and localization of LAT in anergic T cells as a consequence of a selective palmitoylation defect. Immunity *24*, 513–522.

Kalekar, L.A., Schmiel, S.E., Nandiwada, S.L., Lam, W.Y., Barsness, L.O., Zhang, N., Stritesky, G.L., Malhotra, D., Pauken, K.E., Linehan, J.L., et al. (2016). CD4$^+$ T cell anergy prevents autoimmunity and generates regulatory T cell precursors. Nat. Immunol. *17*, 304–314.

Kaye, J., Hsu, M.L., Sauron, M.E., Jameson, S.C., Gascoigne, N.R., and Hedrick, S.M. (1989). Selective development of CD4$^+$ T cells in transgenic mice expressing a class II MHC-restricted antigen receptor. Nature *341*, 746–749.

Kroenke, M.A., Eto, D., Locci, M., Cho, M., Davidson, T., Haddad, E.K., and Crotty, S. (2012). Bcl6 and Maf cooperate to instruct human follicular helper CD4 T cell differentiation. J. Immunol. *188*, 3734–3744.

Labrecque, N., Whitfield, L.S., Obst, R., Waltzinger, C., Benoist, C., and Mathis, D. (2001). How much TCR does a T cell need? Immunity *15*, 71–82.

Lahl, K., Loddenkemper, C., Drouin, C., Freyer, J., Arnason, J., Eberl, G., Hamann, A., Wagner, H., Huehn, J., and Sparwasser, T. (2007). Selective depletion of Foxp3$^+$ regulatory T cells induces a scurfy-like disease. J. Exp. Med. *204*, 57–63.

Laidlaw, B.J., Craft, J.E., and Kaech, S.M. (2016). The multifaceted role of CD4$^+$ T cells in CD8$^+$ T cell memory. Nat. Rev. Immunol. *16*, 102–111.

Laman, J.D., Claassen, E., and Noelle, R.J. (2017). Functions of CD40 and Its ligand, gp39 (CD40L). Crit. Rev. Immunol. *37*, 371–420.

Lercher, A., Bhattacharya, A., Popa, A.M., Caldera, M., Schlapansky, M.F., Baazim, H., Agerer, B., Gürtl, B., Kosack, L., Májek, P., et al. (2019). Type I Interferon signaling disrupts the hepatic urea cycle and alters systemic metabolism to suppress T cell function. Immunity *51*, 1074–1087.e9.

Li, Q., Skinner, P.J., Ha, S.J., Duan, L., Mattila, T.L., Hage, A., White, C., Barber, D.L., O'Mara, L., Southern, P.J., et al. (2009). Visualizing antigen-specific and infected cells in situ predicts outcomes in early viral infection. Science *323*, 1726–1729.

Liu, X., Wang, Y., Lu, H., Li, J., Yan, X., Xiao, M., Hao, J., Alekseev, A., Khong, H., Chen, T., et al. (2019). Genome-wide analysis identifies NR4A1 as a key mediator of T cell dysfunction. Nature *567*, 525–529.

Lynn, R.C., Weber, E.W., Sotillo, E., Gennert, D., Xu, P., Good, Z., Anbunathan, H., Lattin, J., Jones, R., Tieu, V., et al. (2019). c-Jun overexpression in CAR T cells induces exhaustion resistance. Nature *576*, 293–300.

Macián, F., García-Cózar, F., Im, S.H., Horton, H.F., Byrne, M.C., and Rao, A. (2002). Transcriptional mechanisms underlying lymphocyte tolerance. Cell *109*, 719–731.

Magnuson, A.M., Kiner, E., Ergun, A., Park, J.S., Asinovski, N., Ortiz-Lopez, A., Kilcoyne, A., Paoluzzi-Tomada, E., Weissleder, R., Mathis, D., and Benoist, C. (2018). Identification and validation of a tumor-infiltrating Treg transcriptional signature conserved across species and tumor types. Proc. Natl. Acad. Sci. USA *115*, E10672–E10681.

Malherbe, L., Mark, L., Fazilleau, N., McHeyzer-Williams, L.J., and McHeyzer-Williams, M.G. (2008). Vaccine adjuvants alter TCR-based selection thresholds. Immunity *28*, 698–709.

Man, K., Gabriel, S.S., Liao, Y., Gloury, R., Preston, S., Henstridge, D.C., Pellegrini, M., Zehn, D., Berberich-Siebelt, F., Febbraio, M.A., et al. (2017). Transcription factor IRF4 promotes CD8$^+$ T cell exhaustion and limits the development of memory-like T cells during chronic infection. Immunity *47*, 1129–1141.e5.

Mann, T.H., and Kaech, S.M. (2019). Tick-TOX, it's time for T cell exhaustion. Nat. Immunol. *20*, 1092–1094.

Martinez, R.J., Zhang, N., Thomas, S.R., Nandiwada, S.L., Jenkins, M.K., Binstadt, B.A., and Mueller, D.L. (2012). Arthritogenic self-reactive CD4$^+$ T cells acquire an FR4^{hi}CD73^{hi} anergic state in the presence of Foxp3$^+$ regulatory T cells. J. Immunol. *188*, 170–181.

Martinez, G.J., Pereira, R.M., Äijö, T., Kim, E.Y., Marangoni, F., Pipkin, M.E., Togher, S., Heissmeyer, V., Zhang, Y.C., Crotty, S., et al. (2015). The transcription factor NFAT promotes exhaustion of activated CD8$^+$ T cells. Immunity *42*, 265–278.

McKinney, E.F., Lee, J.C., Jayne, D.R., Lyons, P.A., and Smith, K.G. (2015). T-cell exhaustion, co-stimulation and clinical outcome in autoimmunity and infection. Nature *523*, 612–616.

McLane, L.M., Abdel-Hakeem, M.S., and Wherry, E.J. (2019). CD8 T cell exhaustion during chronic viral infection and cancer. Annu. Rev. Immunol. *37*, 457–495.

Mondino, A., Whaley, C.D., DeSilva, D.R., Li, W., Jenkins, M.K., and Mueller, D.L. (1996). Defective transcription of the IL-2 gene is associated with impaired expression of c-Fos, FosB, and JunB in anergic T helper 1 cells. J. Immunol. *157*, 2048–2057.

Moran, A.E., Holzapfel, K.L., Xing, Y., Cunningham, N.R., Maltzman, J.S., Punt, J., and Hogquist, K.A. (2011). T cell receptor signal strength in Treg and iNKT cell development demonstrated by a novel fluorescent reporter mouse. J. Exp. Med. *208*, 1279–1289.

Moreau, H.D., and Bousso, P. (2014). Visualizing how T cells collect activation signals in vivo. Curr. Opin. Immunol. *26*, 56–62.

Morou, A., Brunet-Ratnasingham, E., Dubé, M., Charlebois, R., Mercier, E., Darko, S., Brassard, N., Nganou-Makamdop, K., Arumugam, S., Gendron-Lepage, G., et al. (2019). Altered differentiation is central to HIV-specific CD4$^+$ T cell dysfunction in progressive disease. Nat. Immunol. *20*, 1059–1070.

Myers, D.R., Lau, T., Markegard, E., Lim, H.W., Kasler, H., Zhu, M., Barczak, A., Huizar, J.P., Zikherman, J., Erle, D.J., et al. (2017). Tonic LAT-HDAC7 signals sustain nur77 and Irf4 expression to tune naive CD4 T cells. Cell Rep. *19*, 1558–1571.

Newell, E.W., Ely, L.K., Kruse, A.C., Reay, P.A., Rodriguez, S.N., Lin, A.E., Kuhns, M.S., Garcia, K.C., and Davis, M.M. (2011). Structural basis of specificity and cross-reactivity in T cell receptors specific for cytochrome *c*-I-E$^{(k)}$. J. Immunol. *186*, 5823–5832.

Nguyen, Q.P., Deng, T.Z., Witherden, D.A., and Goldrath, A.W. (2019). Origins of CD4$^+$ circulating and tissue-resident memory T-cells. Immunology *157*, 3–12.

Obst, R. (2015). The timing of T cell priming and cycling. Front. Immunol. *6*, 563.

Obst, R., van Santen, H.M., Mathis, D., and Benoist, C. (2005). Antigen persistence is required throughout the expansion phase of a CD4$^+$ T cell response. J. Exp. Med. *201*, 1555–1565.

Obst, R., van Santen, H.M., Melamed, R., Kamphorst, A.O., Benoist, C., and Mathis, D. (2007). Sustained antigen presentation can promote an immunogenic T cell response, like dendritic cell activation. Proc. Natl. Acad. Sci. USA *104*, 15460–15465.

Okamura, T., Fujio, K., Shibuya, M., Sumitomo, S., Shoda, H., Sakaguchi, S., and Yamamoto, K. (2009). CD4$^+$CD25$^-$LAG3$^+$ regulatory T cells controlled by the transcription factor Egr-2. Proc. Natl. Acad. Sci. USA *106*, 13974–13979.

Oldstone, M.B.A., Ware, B.C., Horton, L.E., Welch, M.J., Aiolfi, R., Zarpellon, A., Ruggeri, Z.M., and Sullivan, B.M. (2018). Lymphocytic choriomeningitis virus Clone 13 infection causes either persistence or acute death dependent on IFN-1, cytotoxic T lymphocytes (CTLs), and host genetics. Proc. Natl. Acad. Sci. USA *115*, E7814–E7823.

Pack, A.D., Collins, M.H., Rosenberg, C.S., and Tarleton, R.L. (2018). Highly competent, non-exhausted CD8$^+$ T cells continue to tightly control pathogen load throughout chronic *Trypanosoma cruzi* infection. PLoS Pathog. *14*, e1007410.

Paley, M.A., Kroy, D.C., Odorizzi, P.M., Johnnidis, J.B., Dolfi, D.V., Barnett, B.E., Bikoff, E.K., Robertson, E.J., Lauer, G.M., Reiner, S.L., and Wherry, E.J. (2012). Progenitor and terminal subsets of CD8$^+$ T cells cooperate to contain chronic viral infection. Science *338*, 1220–1225.

Phan, T.G., Amesbury, M., Gardam, S., Crosbie, J., Hasbold, J., Hodgkin, P.D., Basten, A., and Brink, R. (2003). B cell receptor-independent stimuli trigger immunoglobulin (Ig) class switch recombination and production of IgG autoantibodies by anergic self-reactive B cells. J. Exp. Med. *197*, 845–860.

Philip, M., Fairchild, L., Sun, L., Horste, E.L., Camara, S., Shakiba, M., Scott, A.C., Viale, A., Lauer, P., Merghoub, T., et al. (2017). Chromatin states define tumour-specific T cell dysfunction and reprogramming. Nature *545*, 452–456.

Pradeu, T., and Vivier, E. (2016). The discontinuity theory of immunity. Sci. Immunol. *1*, AAG0479.

Pyke, R.M., Thompson, W.K., Salem, R.M., Font-Burgada, J., Zanetti, M., and Carter, H. (2018). Evolutionary pressure against MHC class II binding cancer mutations. Cell *175*, 416–428.

Qi, H., Cannons, J.L., Klauschen, F., Schwartzberg, P.L., and Germain, R.N. (2008). SAP-controlled T-B cell interactions underlie germinal centre formation. Nature *455*, 764–769.

Quandt, Z., Young, A., Perdigoto, A.L., Herold, K.C., and Anderson, M.S. (2020). Autoimmune endocrinopathies: An emerging complication of immune checkpoint inhibitors. Annu. Rev. Med. *72*, 313–330.

Rabenstein, H., Behrendt, A.C., Ellwart, J.W., Naumann, R., Horsch, M., Beckers, J., and Obst, R. (2014). Differential kinetics of antigen dependency of $CD4^+$ and $CD8^+$ T cells. J. Immunol. *192*, 3507–3517.

Rachmilewitz, J., and Lanzavecchia, A. (2002). A temporal and spatial summation model for T-cell activation: signal integration and antigen decoding. Trends Immunol. *23*, 592–595.

Raziorrouh, B., Sacher, K., Tawar, R.G., Emmerich, F., Neumann-Haefelin, C., Baumert, T.F., Thimme, R., and Boettler, T. (2016). Virus-specific $CD4^+$ T cells have functional and phenotypic characteristics of follicular T-helper cells in patients with acute and chronic HCV infections. Gastroenterology *150*, 696–706.e3.

Reed, J., and Wetzel, S.A. (2019). Trogocytosis-mediated intracellular signaling in $CD4^+$ T cells drives T_H2-associated effector cytokine production and differentiation. J. Immunol. *202*, 2873–2887.

Reeves, P.L.S., Rudraraju, R., Wong, F.S., Hamilton-Williams, E.E., and Steptoe, R.J. (2017). Antigen presenting cell-targeted proinsulin expression converts insulin-specific $CD8^+$ T-cell priming to tolerance in autoimmune-prone NOD mice. Eur. J. Immunol. *47*, 1550–1561.

Richter, K., Brocker, T., and Oxenius, A. (2012). Antigen amount dictates $CD8^+$ T-cell exhaustion during chronic viral infection irrespective of the type of antigen presenting cell. Eur. J. Immunol. *42*, 2290–2304.

Sandu, I., Cerletti, D., Claassen, M., and Oxenius, A. (2020). Exhausted $CD8^+$ T cells exhibit low and strongly inhibited TCR signaling during chronic LCMV infection. Nat. Commun. *11*, 4454.

Saveanu, L., Zucchetti, A.E., Evnouchidou, I., Ardouin, L., and Hivroz, C. (2019). Is there a place and role for endocytic TCR signaling? Immunol. Rev. *291*, 57–74.

Schulze zur Wiesch, J., Ciuffreda, D., Lewis-Ximenez, L., Kasprowicz, V., Nolan, B.E., Streeck, H., Aneja, J., Reyor, L.L., Allen, T.M., Lohse, A.W., et al. (2012). Broadly directed virus-specific $CD4^+$ T cell responses are primed during acute hepatitis C infection, but rapidly disappear from human blood with viral persistence. J. Exp. Med. *209*, 61–75.

Shinkai, Y., Rathbun, G., Lam, K.P., Oltz, E.M., Stewart, V., Mendelsohn, M., Charron, J., Datta, M., Young, F., Stall, A.M., et al. (1992). RAG-2-deficient mice lack mature lymphocytes owing to inability to initiate V(D)J rearrangement. Cell *68*, 855–867.

Snell, L.M., Osokine, I., Yamada, D.H., De la Fuente, J.R., Elsaesser, H.J., and Brooks, D.G. (2016). Overcoming CD4 Th1 cell fate restrictions to sustain antiviral CD8 T cells and control persistent virus infection. Cell Rep. *16*, 3286–3296.

Snell, L.M., McGaha, T.L., and Brooks, D.G. (2017). Type I interferon in chronic virus infection and cancer. Trends Immunol. *38*, 542–557.

Staron, M.M., Gray, S.M., Marshall, H.D., Parish, I.A., Chen, J.H., Perry, C.J., Cui, G., Li, M.O., and Kaech, S.M. (2014). The transcription factor FoxO1 sustains expression of the inhibitory receptor PD-1 and survival of antiviral $CD8^+$ T cells during chronic infection. Immunity *41*, 802–814.

Szymczak-Workman, A.L., Workman, C.J., and Vignali, D.A. (2009). Regulatory T cells do not require stimulation through their TCR to suppress. J. Immunol. *182*, 5188–5192.

Teague, R.M., Greenberg, P.D., Fowler, C., Huang, M.Z., Tan, X., Morimoto, J., Dossett, M.L., Huseby, E.S., and Öhlén, C. (2008). Peripheral $CD8^+$ T cell tolerance to self-proteins is regulated proximally at the T cell receptor. Immunity *28*, 662–674.

Tuncel, J., Benoist, C., and Mathis, D. (2019). T cell anergy in perinatal mice is promoted by T reg cells and prevented by IL-33. J. Exp. Med. *216*, 1328–1344.

van Santen, H.M., Benoist, C., and Mathis, D. (2004). Number of T reg cells that differentiate does not increase upon encounter of agonist ligand on thymic epithelial cells. J. Exp. Med. *200*, 1221–1230.

Vella, L.A., Herati, R.S., and Wherry, E.J. (2017). $CD4^+$ T cell differentiation in chronic viral infections: The Tfh perspective. Trends Mol. Med. *23*, 1072–1087.

Verma, V., Jafarzadeh, N., Boi, S., Kundu, S., Jiang, Z., Fan, Y., Lopez, J., Nandre, R., Zeng, P., Alolaqi, F., et al. (2021). MEK inhibition reprograms $CD8^+$ T lymphocytes into memory stem cells with potent antitumor effects. Nat. Immunol. *22*, 53–66.

Wherry, E.J., Blattman, J.N., Murali-Krishna, K., van der Most, R., and Ahmed, R. (2003). Viral persistence alters CD8 T-cell immunodominance and tissue distribution and results in distinct stages of functional impairment. J. Virol. *77*, 4911–4927.

Wu, C., Nguyen, K.B., Pien, G.C., Wang, N., Gullo, C., Howie, D., Sosa, M.R., Edwards, M.J., Borrow, P., Satoskar, A.R., et al. (2001). SAP controls T cell responses to virus and terminal differentiation of T_H2 cells. Nat. Immunol. *2*, 410–414.

Xu, W., Zhao, X., Wang, X., Feng, H., Gou, M., Jin, W., Wang, X., Liu, X., and Dong, C. (2019). The transcription factor Tox2 drives T follicular helper cell development via regulating chromatin accessibility. Immunity *51*, 826–839.e5.

Yamashiro, H., Hozumi, N., and Nakano, N. (2002). Development of $CD25^+$ T cells secreting transforming growth factor-β1 by altered peptide ligands expressed as self-antigens. Int. Immunol. *14*, 857–865.

Zander, R., Schauder, D., Xin, G., Nguyen, C., Wu, X., Zajac, A., and Cui, W. (2019). $CD4^+$ T cell help is required for the formation of a cytolytic $CD8^+$ T cell subset that protects against chronic infection and cancer. Immunity *51*, 1028–1042.e4.

Zhu, M., Granillo, O., Wen, R., Yang, K., Dai, X., Wang, D., and Zhang, W. (2005). Negative regulation of lymphocyte activation by the adaptor protein LAX. J. Immunol. *174*, 5612–5619.

Zikherman, J., Parameswaran, R., and Weiss, A. (2012). Endogenous antigen tunes the responsiveness of naive B cells but not T cells. Nature *489*, 160–164.

Zinzow-Kramer, W.M., Weiss, A., and Au-Yeung, B.B. (2019). Adaptation by naïve $CD4^+$ T cells to self-antigen-dependent TCR signaling induces functional heterogeneity and tolerance. Proc. Natl. Acad. Sci. USA *116*, 15160–15169.

Zuber, J., and Sykes, M. (2017). Mechanisms of mixed chimerism-based transplant tolerance. Trends Immunol. *38*, 829–843.

STAR★METHODS

KEY RESOURCES TABLE

REAGENT or RESOURCE	SOURCE	IDENTIFIER
Antibodies		
Anti-mouse CD3ε, biotin, clone 145-2C11	Biolegend	Cat#100304; RRID:AB_312669
Anti-mouse CD4, PE, clone GK1.5	Biolegend	Cat#100408; RRID:AB_312693
Anti-mouse CD4, PerCP-Cy5.5, clone RM4-5	eBioscience	Cat#45-0042-82; RRID:AB_1107001
Anti-mouse CD4, PE-Cy7, clone GK1.5	Biolegend	Cat#100422; RRID:AB_312707
Anti-mouse CD4, biotin, clone RM4-5	Biolegend	Cat#100508; RRID:AB_312711
Anti-mouse CD8α, biotin, clone 53-6.7	Biolegend	Cat#100704; RRID:AB_312743
Anti-mouse CD8α, FITC, clone 53-6.7	Biolegend	Cat#100706; RRID:AB_312745
Anti-mouse CD11b, biotin, clone M1/70	Biolegend	Cat#101204; RRID:AB_312787
Anti-mouse CD11b, PE-Cy7, clone M1/70	Biolegend	Cat#101216; RRID:AB_312799
Anti-mouse CD11c, biotin, clone N418	Biolegend	Cat#117304; RRID:AB_313773
Anti-mouse CD11c, PerCP, clone N418	Biolegend	Cat#117326; RRID:AB_2129643
Anti-mouse CD16/32, unlabeled, clone 2.4G2	Bio X Cell	Cat#BE0008; RRID:AB_1107603
Anti-mouse CD19, AL647, clone 6D5	Biolegend	Cat#115522; RRID:AB_389329
Anti-mouse CD40, clone FGK45.5	BioXcell	Cat#BE0016-2; RRID:AB_1107647
Anti-mouse CD44, FITC, clone IM7	Biolegend	Cat#103006; RRID:AB_312957
Anti-mouse CD44, PE-Cy7, clone IM7	Biolegend	Cat#103030; RRID:AB_830787
Anti-mouse CD45.1, FITC, clone A20	Biolegend	Cat#110706; RRID:AB_313495
Anti-mouse CD45.1, PerCP, clone A20	Biolegend	Cat#110726; RRID:AB_893345
Anti-mouse CD45.1, PE-Cy7, clone A20	Biolegend	Cat#110730; RRID:AB_1134168
Anti-mouse CD45.1, APC, clone A20	Biolegend	Cat#110714; RRID:AB_313503
Anti-mouse CD45R, PE, clone RA3-6B2	Biolegend	Cat#103208; RRID:AB_312993
Anti-mouse CD45R, PE-Cy7, clone RA3-6B2	Biolegend	Cat#103222; RRID:AB_313005
Anti-mouse CD49b, biotin, clone DX5	Biolegend	Cat#108904; RRID:AB_313411
Anti-mouse CD62L, PE, clone MEL-14	Biolegend	Cat#104408; RRID:AB_313095
Anti-mouse CD69, PE, clone H1.2F3	Biolegend	Cat#104508; RRID:AB_313111
Anti-mouse CD73, PE, clone TY/11.8	Biolegend	Cat#127206; RRID:AB_2154094
Anti-mouse CD90.1, FITC, clone HIS51	eBioscience	Cat#11-0900-81; RRID:AB_465151
Anti-mouse CD90.1, PerCP, clone OX7	Biolegend	Cat#202512; RRID:AB_1595487
Anti-mouse CD90.2, PE, clone 30-H12	Biolegend	Cat#105308; RRID:AB_313179
Anti-mouse CD127, PE, clone A7R34	eBioscience	Cat#12-1271-81; RRID:AB_465843
Anti-mouse CD134, PE, clone Ox-86	Biolegend	Cat#119409; RRID:AB_2272150
Anti-mouse CD137L, PE, clone TKS-1	Biolegend	Cat#107105; RRID:AB_2256408
Anti-mouse CD154, PE, clone MR1	Biolegend	Cat#106506; RRID:AB_313271
Anti-mouse CD185, PE, clone L13D7	Biolegend	Cat#145503; RRID:AB_2561967
Anti-mouse CD200, PE, clone OX-90	Biolegend	Cat#123907; RRID:AB_2074081
Anti-mouse CD218a, PE, clone P3TUNYA	eBioscience	Cat#12-5183-80; RRID:AB_2572616
Anti-mouse CD223, biotin, clone C9B7W	Biolegend	Cat#125205; RRID:AB_961177
Anti-mouse CD244.2, FITC, clone m2B4	Biolegend	Cat#133503; RRID:AB_1595624
Anti-mouse CD278, FITC, clone C398.4A	Biolegend	Cat#313506; RRID:AB_416330
Anti-mouse CD279, PE-Cy7, clone RMP1-30	Biolegend	Cat#109109; RRID:AB_572016
Anti-mouse CD366, PE, clone RMT3-23	Biolegend	Cat#119703; RRID:AB_345377)
Anti-mouse c-Maf, PE, clone symOF1	eBioscience	Cat#12-9855-41; RRID:AB_2572746
Anti-mouse Foxp3, eFluor® 660, clone FJK-16 s	eBioscience	Cat#50-5773-82; RRID:AB_11218868

(*Continued on next page*)

Continued

REAGENT or RESOURCE	SOURCE	IDENTIFIER
Anti-mouse FR4, PE-Cy7, clone eBio12A5	Biolegend	Cat#25-5445-82; RRID:AB_842811
Anti-mouse IFNγ, APC, clone XMG1.2	Biolegend	Cat#505810; RRID:AB_315404
Anti-mouse IL-2, PE-Cy7, clone JES6-5A4	eBioscience	Cat# 25-7021-82 ; RRID:AB_1235004
Anti-mouse IRF4, PE, clone IRF4.3E4	Biolegend	Cat#646403; RRID:AB_2563004
Anti-mouse LAT, unconjugated, clone E3U6J	Cell Signaling	Cat#9166S; RRID:AB_2283298
Anti-mouse Ly-6C, FITC, clone HK1.4	Biolegend	Cat#128006; RRID:AB_1186135
Anti-mouse NFATc1, Al488, clone 7A6	Biolegend	Cat#649604; RRID:AB_2561823
Anti-p-c-Jun, PE, clone MK-1	Santa Cruz	Cat#sc-822 PE; RRID:AB_627262
Anti-p-S6, Al488, clone 2F9	Cell Signaling	Cat#4854 S;RRID:AB_390782
Anti-mouse Siglec H, PE, clone 551	Biolegend	Cat#129606; RRID:AB_2189147
Anti-mouse TCRβ, FITC, clone H57-597	Biolegend	Cat#109206; RRID:AB_313429
Anti-mouse TCRβ, biotin, clone H57-597	Biolegend	Cat#109203; RRID:AB_313426
Anti-mouse TCRγδ, biotin, clone UC7-13D5	eBioscience	Cat#13-5811-85; RRID:AB_466685
Anti-mouse TCR-Vα11, biotin, clone PR8-1	BD	Cat#553221; RRID:AB_394716
Anti-mouse TCR-Vβ3, FITC, clone KJ25	CBDM Labs	N. Asinovski, C. Benoist, D. Mathis
Anti-mouse TCR-Vβ3, BV650, clone KJ25	BD	Cat#743415; RRID:AB_2741488
Anti-mouse Ter119, biotin, clone TER-119	Biolegend	Cat#116204; RRID:AB_313705
Anti-mouse TIGIT, PE, clone 1G9	Biolegend	Cat#142103; RRID:AB_10895760
Anti-mouse TNFα, FITC, clone MP6-XT22	Biolegend	Cat#506304; RRID:AB_315425
Anti-mouse TOX, PE, clone TXRX10	eBioscience	Cat# 12-6502-82; RRID:AB_10855034
Chemicals and peptides		
Antibiotic/Antimycotic Solution	PAA	Cat#P11-002
Cytofix Buffer	BD Bioscience	Cat#554655
Phosflow PermBuffer III	BD Bioscience	Cat#558050
Bovine serum albumin (BSA), Fraction V	Thermo Fisher	Cat#11413164
Brefeldin A	Sigma Aldrich	Cat#20350-15-6
CellTrace Violet	Thermo Fisher	Cat#C34557
Chloroform	Carl Roth	Cat#67-66-3
DAPI (4,6-diamidino-2-phenylindole)	Invitrogen	Cat#D1306
Dimethyl sulfoxide (DMSO)	Thermo Fisher	Cat#67-68-5
DMEM	Applichem	Cat#A1316
DNase I from bovine pancreas	Roche	Cat#11284932001
Doxycycline (Beladox)	Bela-Pharm	Cat#793-588
FCS (GIBCO)	Life Technologies	Cat#10438018
Foxp3/Transcription Factor staining buffer set	eBioscience	Cat#00-5523-00
Ficoll (Pancoll human)	PAN Biotech	Cat#P04-60500
Fixable Viability Dye eFlour 450	eBioscience	Cat#65-0863-14
Fixable Viability Dye eFlour 660	eBioscience	Cat#65-0864-14
Fixable Viability Dye eFlour 780	eBioscience	Cat#65-0865-14
Fluo-4, AM, cell permeant	Thermo Fisher	F14201
Fura Red, AM, cell permeant	Thermo Fisher	F3020
Hen egg lysozyme (HEL)	Sigma Aldrich	Cat#A3711
HEPES Buffer Solution (1 M)	PAA	Cat#S11-001
Intracellular Fixation & Permeabilization Buffer Set	eBioscience	Cat#88-8824-00
Ionomycin (IM)	Diagonal	Cat#56092-82-1
L-Glutamine (PAA)	GE Healthcare	Cat#11541911
Liberase	Roche	Cat#5401119001
Linear polyacrylamide (GeneElute)	Sigma Aldrich	Cat#1001854941

(*Continued on next page*)

Continued

REAGENT or RESOURCE	SOURCE	IDENTIFIER
peptides MCC_{88-103}, MCC_{93-103}	Peptides & Elephants	Custom
Phorbol myristate acetate (PMA)	Sigma-Aldrich	Cat#16561-29-8
RPMI 1640 Medium, Glutamax Supplement	Thermo Fisher	Cat#61870010
Sigma Adjuvant System (Ribi)	Sigma Aldrich	Cat# S6322
Streptavidin (PE)	Biolegend	Cat#405203
Streptavidin (APC-Cy7)	Biolegend	Cat#405208
Streptavidin (PE-Cy7)	Biolegend	Cat#405206
Trizol LS reagent	Life Technologies	Cat#10296028
Critical commercial assays		
Agilent RNA 6000 Pico	Agilent	Cat#5067-1511
Brilliant III Ultra-Fast SYBR Green QPCR	Agilent	Cat#600882
MACS anti-biotin MicroBeads	Miltenyi	Cat#130-090-485
MACS LS Columns	Miltenyi	Cat#130-042-401
Mouse Gene 2.0 ST Microarrays	Affymetrics	Cat#902119
NucleoSpin RNA Clean-up XS	Macherey-Nagel	Cat#740903.50
Ovation Pico WTA System V2 cDNA Amplification Kit	Nugen	Cat#3302-A01
Encore Biotin Module for Fragmentation and Labeling cDNA	Nugen	Cat#4200-A01
rDNase set	Macherey-Nagel	Cat#740963
SuperScript III First-Strand Synthesis System	Invitrogen	Cat#18080-051
Deposited data		
Microarray transcriptomic data	This study	GEO: GSE143739
Experimental models: organisms/strains		
Mouse: B10.BR or	Jackson	B10.BR-$H2^{k2}$ $H2\text{-}T18^{a}$/SgSnJJrep, Jackson stock no. 004804
Mouse: B10.BR	Harlan/Envigo	B10.BR-H-2^{k}/OlaHsd
Mouse: AND	Obst et al., 2005	B10.BR-Tg(TcrAND)53Hed
Mouse: CD45.1	Obst et al., 2005	B10.BR-$Ptprc^{a}$
Mouse: $SAP^{o/o}$	Wu et al., 2001	B10.BR-$Sh2d1a^{tm1Cpt}$
Mouse: $RAG2^{o/o}$	Shinkai et al., 1992	B10.BR-$RAG2^{tm1Fwa}$
Mouse: Ii-rTA	Obst et al., 2005	B10.BR-Tg(Cd74-rtTA)#Doi
Mouse: TIM	van Santen et al., 2004	B10.BR-Tg(tetO-Cd74/MCC)#Doi
Mouse: cMCC	Yamashiro et al., 2002	B10.BR-Tg(H2-Ea-Cd74/MCC)37GNnak
Mouse: NR4a1-EGFP	Moran et al., 2011	B10.BR-Tg(Nr4a1-EGFP/cre)820Khog, Jackson stock no. 016617
Mouse: SW_{HEL}	Phan et al., 2003	B10.BR-Igh^{tm1Rbr}-Tg(IgkHyHEL10)1Rbr
Mouse: FoxP3-EGFP	Lahl et al., 2007	Tg(Foxp3-DTR/EGFP)23.2Spar
Oligonucleotides		
GGATCCTGAGAACTTCAGGctc	Obst et al., 2005	rabbit β-globin-FW
TGATGAGACAGCACAACAACC	Obst et al., 2005	rabbit β-globin REV
GACGGCCAGGTCATCACTATTG		mouse β-actin-FW
AGGAAGGCTGGAAAAGAGCC		mouse β-actin-REV
Software and algorithms		
Affinity Designer 1.8.4	Affinity	https://affinity.serif.com:443/
FlowJo 10.4.2	FlowJo	https://www.flowjo.com
GraphPad Prism 7	GraphPad Software	https://www.graphpad.com

(*Continued on next page*)

Continued

REAGENT or RESOURCE	SOURCE	IDENTIFIER
IDEAS 6.2	Merck KGaA	https://www.emdmillipore.com/US/en
MultiplotStudio 1.5.20	SP Davis & C. Benoist, HMS	http://gparc.org

RESOURCE AVAILABILITY

Lead contact

Further information and requests for resources and reagents should be directed to and will be fulfilled by the Lead Contact, Reinhard Obst (reinhard.obst@med.uni-muenchen.de).

Materials availability

This study did not generate new unique reagents.

Data and code availability

The accession number for the microarray data reported in this paper is GEO: GSE143739. This study did not generate unique code.

EXPERIMENTAL MODEL AND SUBJECT DETAILS

Mice

B10.BR mice were purchased from Jackson Laboratories (B10.BR-*H2*^{k2} *H2-T18*^{a}/SgSnJJrep, stock number 004804) or Harlan, now Envigo (B10.BR-H-2^{k}/OlaHsd). All transgenes and deleted loci were backcrossed to the B10.BR-H-2^{k} background. iMCC animals carry the transgenes Ii-rTA (Obst et al., 2005; Tg(Cd74-rtTA)#Doi) and TIM (van Santen et al., 2004; Tg(tetO-Cd74/MCC)#Doi, cMCC animals carry a tg Ii-MCC$_{88\text{-}103}$ fusion protein under the control of the H-2Eα promoter (Yamashiro et al., 2002; Tg(H2-Ea-Cd74/MCC)37GNnak). AND TCR tg mice (Kaye et al., 1989) carry the CD45.1 allogenic marker for identification which was originally derived from B6.SJL-Ptprc^{a}Pepd^{b}/BoyJ animals (Han et al., 2010). For transcriptome analyses, AND tg with Ptprc^{a} and Rag2$^{o/o}$ loci were used. NR4a1-EGFP tg (Tg(Nr4a1-EGFP/cre)820Khog) were purchased from The Jackson Laboratories (stock no. 016617) and backrossed to the AND, Ptprc^{a} and the H-2$^{k/k}$ loci. SAP$^{o/o}$ animals (Wu et al., 2001; Sh2d1a^{tm1Cpt}) and SW$_{HEL}$ animals (Phan et al., 2003; Igh^{tm1Rbr}-Tg(IgkHyHEL10)1Rbr) were provided by M. Turner, Babraham Institute, Cambridge, UK, and backcrossed to carry the cMCC, Ptprc$^{a/a}$ and H-2$^{k/k}$ loci. Mice of both sexes were used at 6-16 weeks of age. All mice were genotyped by PCR and housed in groups of 2-5 animals per cage in specific pathogen-free facilities at the Institute for Immunology or at the specific and opportunistic pathogen free facilities of the Core Facility Animal Models at the Biomedical Center of the Ludwig-Maximilians-Universität Munich. All protocols were approved by the Government of Upper Bavaria, protocol no. 55.2-1-54-2532-84-2015.

METHOD DETAILS

Animal Treatments and Adoptive Transfers

Single cell suspensions were prepared in FACS buffer (DMEM/5 mM HEPES/1% BSA) from axillary, brachial, and inguinal lymph nodes from donor AND^{+}CD45.1 animals (6-20 weeks, females) with microscopic glass slides and checked for the presence of 50%–60% of naive (CD44l$^{ow/int}$ CD62L^{high}) TCR-Vβ3^{+} CD4^{+} T cells.

Recipient animals (6-20 weeks, both sexes) were injected i.p. with 20 μg of the agonistic anti-CD40 mAb FGK45.5 (Obst et al., 2007) on day −1 and were injected i.v. with 10^{6} lymph node cells from AND^{+}CD45.1 animals in 100 μl DMEM, except those in Figures 1A–1C and the control recipients 1-3 in Figure 7B. Control recipients (B10.BR or untreated iMCC) were injected with lymph node cells 3 days before sacrifice since AND T cells wane in the absence of antigen, as has been observed for several CD4^{+} TCR tg T cells (Hataye et al., 2006; Obst et al., 2007). All donor cells were routinely checked for viability (> 95% DAPI^{-}), TCR Vβ3 and CD44$^{low/int}$CD62L^{+} naive phenotype before transfer. iMCC animals were put on water low in divalent cations (Volvic or desalinated water) containing 100 μg/mL dox (Bela-Pharm) on day −1, were kept on it or switched to normal water or 10 μg/ml on day 3 as indicated. Experiments were terminated by the sacrifice of the recipients by CO_2 asphyxiation or cervical dislocation.

For secondary transfers (Figure 6D), axillary, brachial, and inguinal lymph nodes of primary recipients were removed and pooled from 1-3 animals. Single cells suspensions were incubated with biotinylated mAbs against CD8, CD11b, CD11c, CD45R, CD49b, GR-1 and TER119, washed twice in FACS medium, incubated with anti-biotin beads and depleted of the respective populations by passing them over magnetized LS columns (Miltenyi). The flow-through contained > 90% CD4^{+} T cells. 5x10^{6} cells were injected i.v. into secondary hosts.

For *in vivo* peptide challenges (Figure 3G), recipient animals were injected with 100 μl PBS or with 25 μg MCC_{88-103} in 100 μl PBS i.v. 1 hour before sacrifice. Splenocytes were resuspended in FACS buffer immediately, fixed in prewarmed Cytofix buffer (added 1:1) and incubated at 37°C for 10 minutes. Cells were washed in FACS buffer and permeabilized by slow addition of 0.5 mL of −20°C cooled Perm buffer III to the slowly vortexed cells and an incubation on ice for 30 minutes. Cells were then stained in FACS buffer at room temperature.

For B cell experiments (Figure 7B) $5x10^6$ $CD45R^+$ spleen B cells from B10.BR-SW_{HEL}-cMCC-CD45.1 animals were i.v. injected. The AND cells in these experiments carried the CD90.1 congenic marker.

For immunizations (Figure S1B) animals were subcutaneously injected with 60 μg MCC_{93-103} in Ribi adjuvant and analyzed 7-8 days later (Fazilleau et al., 2009).

CTV Labeling

$20x10^6$ LN cells per ml were resuspended in Ca^{2+}/Mg^{2+}-free PBS/0.1% BSA at 37°C and 2 μl/ml of 5 mM CTV in DMSO were added while the cells were vigorously vortexed. Cells were incubated at 37°C for 10 minutes before the cells were centrifuged through a cushion of FCS, washed in DMEM and resuspended at $10x10^6$ cells per ml for adoptive transfer.

Flow Cytometry: Standard Stainings

Splenocytes single cell suspensions were prepared with glass microscopy slides in FACS buffer, filtered through a 70 μm^2 mesh and red blood cells were separated by a centrifugation through a Ficoll cushion at 670 *rcf.* for 15 minutes with reduced deceleration. The cells were washed and $3-5x10^6$ cells were aliquoted into round bottom 96-well plates. Cells were centrifuged and resuspended in 50 μl of FACS buffer containing mAbs listed in the Reagents list, including 2.5 μg of the FcγR blocking mAb anti CD16/32 2.4G2. The cells were centrifuged, resuspended in FACS buffer and read out in BD Canto II or BD Fortessa Analyzers. Open histograms show isotype control stainings.

Cytokines

$4x10^6$ splenocytes were stimulated in round bottom 96-well plates with 20 ng/ml PMA and 1 μg/ml IM in RPMI-Glutamax/10% FCS/ 50 μM 2-ME/100 units/ml penicillin/0.1 mg/ml streptomycin/0.25 μg amphotericin B for 4 hours with 10 μg/ml Brefeldin A added for the last 2. The cells were harvested and stained with Fixable Viability Dye eFluor 450, 660 or 780 (1:1000 in PBS) and antibodies for 15 minutes at 4°C and cytokines were stained with the eBioscience Intracellular Fixation & Permeabilization Buffer Set as per manufacturer's instructions.

Phosphorylated Proteins

For intracellular visualization of P-S6 splenocytes were resuspended in FACS buffer immediately after sacrifice, fixed in 37°C prewarmed 4% PFA at 37°C for 10 minutes. Cells were washed in FACS buffer and permeabilized by the slow addition of 0.5 mL of −20°C cooled Perm buffer III to the slowly vortexed cells and an incubation on ice for 30 minutes. Cells were then washed and stained in FACS buffer at room temperature. For stainings of P-Jun splenocytes were washed and then fixed with 2% PFA for 20 minutes at room temperature. The cells were then washed with PBS and incubated with Fcγ blocking mAb for 15 minutes at RT and then washed twice with PBS/2% FCS/0.2% sodium azide and then twice with the same buffer containing 0.5% saponin and stained for 30 minutes, washed sequentially in permeabilization and staining buffers and measured.

NFAT Localization

For the analysis of NFATc1/Draq5 co-localization, splenocyte single cell suspensions were prepared immediately after sacrifice and fixed by adding 4% paraformaldehyde 1:1, an incubation at room temperature for 10 min, washed and resuspended in permeabilization buffer (eBioscience). The cells were stained with indicated antibodies and Draq5 and analyzed by using an $ImageStream^X$ MKII cytometer. Nuclear translocation of NFATc1 was determined using the similarity feature in the IDEAS software. A similarity score was defined that measures the correlation of pixel co-localization between the Draq5 and NFATc1 images of each cell.

Ca^{2+} Responsiveness

Splenocytes were enriched for $CD4^+$ T cells by incubations with biotinylated mAbs against CD8, CD11b, CD11c, CD45R, CD49b, GR-1 and TER119, two washes in FACS medium, incubation with anti-biotin beads and depletion of the respective populations by passing them over magnetized LS columns (Miltenyi). The flow-through contained > 90% $CD4^+$ T cells. 10^6 cells were resuspended in 500 μl complete RPMI/1% BSA medium and incubated at 37°C. The Ca^{2+}-sensitive dyes Fluo-4 and Fura-Red, the 1 mM and 3 mM frozen stock solutions in DMSO were thawed and diluted in RPMI/1% BSA to yield a 2x labeling solution (2 μM Fluo-4, 6 μM FuraRed) which was added to the cells while vortexed to ensure homogeneous dye loading. The cells were incubated for 30-60 minutes at 37°C with occasional mixing. The cells were washed twice with FACS medium without BSA at room temperature and a small sample put aside as a compensation control. The pellet was resuspended in 200 μl medium with 3 μl biotinylated anti-CD3ε, 3 μl biotinylated anti-CD4, and 1 μl anti-CD45.1 for cell identification, incubated for 15 minutes at room temperature, washed twice and resuspended in 500 μl FACS buffer. During data acquisition at the BD FACSCanto II over 5 minutes samples were spiked with 20 μg SA after 1 minute and 100 ng IM after 4 minutes.

Cell Sorting

For APC analyses, spleens of two mice were digested with 0.9 mg/ml liberase/0.2 mg/ml DNase in DMEM for 10 minutes at 37°C, washed and red blood cells were separated by a centrifugation through a Ficoll cushion at 670 *rcf.* for 15 minutes with reduced deceleration. Cells were depleted of T, B, and NK cells, granulocytes and erythroid precursors by incubation with biotinylated mAbs (TCRβ, TCRγδ, CD19, CD49b, GR-1 and Ter119) and anti-biotin MACS beads and separated over magnetized LS columns (Miltenyi). The cells were then stained as indicated in Figure S1A and sorted with a BD FACSAria III sorter.

For transcriptomic analyses, single cell suspensions of lymph node and spleen cells of recipient animals were pooled and incubated with biotinylated antibodies against CD8, CD11b, CD11c, CD45R, CD49, Gr-1 and TER119. Washed cells were then incubated with anti-biotin microbeads and depleted by passing them over magnetized LS columns (Miltenyi). The resulting $CD4^+$ cell suspensions were stained and sorted twice as SA^- $CD4^+CD45.1^+CD90.2^+TCRV\beta3^+DAPI^-$ singlets on a Beckmann Coulter MoFlo XDC sorter. The yield of test sorts was > 99% purity. The cells of the second sort were sorted directly into 500 μl Trizol LS, mixed and stored at −80°C for processing. Five independent replicates per condition were generated.

For transcriptomic analyses of anergic and control cells, B10.BR lymph node and spleen cells were pooled and out of the $DAPI^-CD4^+CD44^{high}$ singlets, $CD73^+FR4^+$ and $CD73^-FR4^-$ were sorted from five mice.

Quantitative RT-PCR: Assessment of Transgene Expression

RNA from sorted APC populations were isolated with Trizol LS and cDNA synthesized with Superscript III (Invitrogen) and oligo-dT per manufacturer's protocol. The common rabbit β-globin splice substrate of the iMCC and cMCC transgenes (gray in Figure 1A) and mouse β-actin were quantified with a SYBR green master mix (Agilent) and the primers listed in the Key Resources Table. Data were displayed as fold change (FC) = $2^{-(Ct[\beta\text{-globin}]-Ct[\beta\text{-actin}])}$.

Transcriptome Analysis: RNA Isolation

The Trizol samples were thawed on ice, 300 μl chloroform was added, shaken, incubated for 3 minutes at room temperature and spun at 12,000 x g and 4°C. The aqueous phase was transferred to new tubes, 1 volume of isopropanol and 1 μl of linear polyacrylamide stock solution (25 μg/μl) was added. The samples were precipitated for 16 hours at −20°C and centrifuged for 10 minutes at 12,000 x g and 4°C. Supernatants were removed and RNA pellets washed with 70% ethanol. RNA pellets were resuspended in 100 μl RNase-free water and purified with NucleoSpin RNA Clean-up XS columns as per manufacturer's instructions, from which the RNA was eluted with 12 μl water and stored at −80°C. RNAs were quantified with an Agilent 2100 Bioanalyzer. All samples had RNA integrity values > 8 and were used for amplification and microarray hybridizations.

Expression Profiling

Total RNA (0.1-30 ng) was amplified and labeled using the Ovation Pico WTA System V2 in combination with the Encore Biotin Module (Nugen). Amplified cDNA was hybridized on Affymetrix Mouse Gene 2.0 ST arrays containing about 35,000 probe sets. Staining and scanning using a GeneChip Scanner 3000 7G was done according to the Affymetrix expression protocol including minor modifications as suggested in the Encore Biotin protocol.

QUANTIFICATION AND STATISTICAL ANALYSIS

Cytometry Data Analysis

Data were analyzed with the FlowJo software. Extracted expression levels were assessed for normality with the Shapiro-Wilk test of the Prism software. Data were plotted and tested with the Prism software and statistical tests used as indicated in the figure legends. Statistics panels depict data points and means.

Transcriptomic Data Analysis

Data normalization and background correction was performed in R using Robust Multichip Average (RMA, library 'oligo') including background correction and quantile normalization. Technical control probe sets as well as probe sets with zero variance were removed. Samples which did not pass quality control (package 'arrayQualityMetrics', version 3.32.0; 1 day-10 T^{int}, 1 day-10 T^{high}) were excluded from further analysis. Furthermore, only probe sets exhibiting a log2 expression value of > 4 in at least one condition were considered for further analyses. Many-probe-sets-to-one-gene relationships were resolved by keeping only one probe set with highest variance for each gene (annotation package 'mogene20sttranscriptcuster.db'). Differentially expressed genes were identified using a moderated t-statistic (R package 'limma'). Transcription factors binding site enrichment was determined using 'RcisTarget' and motif database 'mm9_10kbpAroundTss_motifRanking' within the R package 'RcisTarget.mm9.motifDatabases.20k.' NES threshold was 3. Gene set enrichment analyses were conducted using mroast ('limma' package) with 10000 rotations. GO and KEGG pathway enrichment analyses were performed using a hypergeometric distribution test as supplied by the 'GOstats' package using a p value cutoff of 0.001. Data were visualized as heatmaps, FC/FC and volcano plots using MultiplotStudio 1.5.20 available at the GenePattern Archive (http://gparc.org).